ASSESSMENT OF PELLET INJECTION FOR NET

PART V:

Ignition and fuelling scenario calculations

L.L.Lengyel

IPP 1/236 August 1985

MAX-PLANCK-INSTITUT FÜR PLASMAPHYSIK

8046 GARCHING BEI MÜNCHEN

MAX-PLANCK-INSTITUT FÜR PLASMAPHYSIK

GARCHING BEI MÜNCHEN

ASSESSMENT OF PELLET INJECTION FOR NET
PART V:
Ignition and fuelling scenario calculations

L.L.Lengyel

IPP 1/236 August 1985

Die nachstehende Arbeit wurde im Rahmen des Vertrages zwischen dem Max-Planck-Institut für Plasmaphysik und der Europäischen Atomgemeinschaft über die Zusammenarbeit auf dem Gebiete der Plasmaphysik durchgeführt.

Abstract

Results of ignition and continuous fuelling scenario calculations are presented that were obtained in the framework of an assessment performed for NET on the basis of the INTOR parameters. The results obtained with pellet injection are compared with results corresponding to gas puffing.
Pellet injection transports fresh fuel to the reaction zone on a time scale that is much shorter than the diffusion time characterizing the gas puffing method, thus making the method flexible and readily adaptable to different situations.
In the case of ignition by pellet injection, it may become possible to have deep NB penetration and maintain favourable heat deposition profiles up to the moment of density ramp-up, thus substantially relaxing the beam output requirements.
Three beam energies (D^o particles) have been considered: 120 keV, 100 keV, and 80 keV. The importance of a proper match between the beam characteristics and the pellet parameters, specific for the transport scaling assumed (ALCATOR-INTOR), is shown. In the case of continuous fuelling of an already ignited discharge, the alpha power production notably increases if repetitive pellet injection, instead of gas puffing (at a fixed value of β_T), is applied. The advantages of pellet injection are substantial even at moderate pellet velocities.

1. Introduction

Pellet injection is considered to be a potential candidate for some fundamental applications in fusion devices, such as ignition by means of density ramp-up and fuelling of an already ignited discharge by repetitive pellet injection. Several recent tokamak experiments have demonstrated some of the potentials pellet injection may have: a substantial improvement of the energy confinement time was obtained with the help of pellets in ALCATOR-C /1/ and in Doublet III /2/, and a notable short-time increase of the plasma density over the density limit was observed after pellet injection in PDX /3/. The plasma physical results obtained with pellet injection seem to depend strongly on experimental conditions and discharge regimes investigated: experiments performed on other tokamaks (TFTR, ASDEX /4/) have not yet been able to reproduce the encouraging results of /1/ and /2/.

In view of the developments in the field of pellet injection in tokamaks it was decided to assess its applicability to large-scale fusion devices such as NET /5/. The results of scenario calculations performed in the framework of /5/ are reported herein. In particular, scenarios associated with density ramp-up and ignition by means of single pellets and quasi-continuous fuelling of already ignited discharges by repetitive injection of a string of pellets are considered in detail.

Earlier ignition scenario analyses applied to NB-heated tokamaks (see , for example, /6/ to /8/) demonstrated the importance of proper matching between the fuel density and heat deposition profiles both in space and time. Watkins et al. /6/ showed that there is an optimum route to ignition in the n,T space bounded on the low-density side by electron conduction losses (ALC.-INT. scaling) and by poor beam penetration on the high-density side. They showed that, independently of the fixed density profile approximation

used in their computations, the minimum beta necessary for ignition always occurs at low densities. Holmes et al. /7/ considered low-density ignition scenarios, starting in all cases with $n(r = o) = 8 \times 10^{19}$ m^{-3} and modelling continuous (pellet) fuelling by a source distribution that was flat in the outer 25 cm of a a = 1.25 m reactor plasma and then decayed exponentially inward with an e-folding length of 5 cm. A single-temperature 1-D transport code coupled to a 2-D flux-conserving equilibrium code was used in these calculations. The results show that with a transport scaling $\tau_E \propto n$ it is advantageous to start beam injection in a plasma with low $n \cdot a$ and then to increase the density n (or plasma size a) to reach ignition. It was found to be favourable to fuel as rapidly as possible without creating significant density inversion. Houlberg et al. /8/ performed extensive scenario calculations for FED also by applying the ALC.-INT. transport scaling to beam-heated discharges. Owing to the density dependence of the NB heat deposition profile, notable differences were found in the actual behaviour of the resulting energy confinement time and that expected from global scaling law analysis. The results of /8/ clearly show the importance of a proper match between the envisaged energy influx rate and deposition profile, on the one hand, and the particle source strength and distribution, on the other, when heating by NB injection is considered.
The purpose of the present work is to explore in this context the new possibilities offered by pellet injection in conjunction with NB injection heating of fusion plasmas. The flexibility of fuel deposition profiles associated with different pellet size-velocity-injection frequency combinations and the possibility of matching these characteristics with the beam properties may contribute to improved performance characteristics of fusion systems. Two major objectives have been considered in detail: (a) the possibility of fast density ramp-up with the help of pellets and the associated reduction of the NB performance requirements; (b) a possible increase of the alpha power production (at constant β_T) due to the favourable density and temperature profiles produced by pellet injection.

2. Reference Discharge and Transport Model

In all transport calculations reported herin the BALDUR 1-D radial transport code /9/ has been applied. The parameters of the recipient discharge were chosen in accordance with INTOR specifications ($r = 5.2$ m, $a = 1.6$ m, $b/a = 1.6$, $B_z = 5.5$ tesla, $I = 6.4$ MA). The scrape-off version of BALDUR used has allowed the ions diffusing to the scrape-off layer and entering the divertor slits to be pumped off. To simulate the intense localized recycling of the hydrogen in the divertor chamber expected unter INTOR conditions the parallel flow Mach number in the scrape-off layer was assumed to be 0.02. The wall recycling coefficient was assumed to be unity, i.e. all thermal plasma particles reaching the wall were returned to the plasma as neutrals with an energy of 3 eV. The energetic cx neutrals lost were not included in the number of recycled particles: they were replaced by gas puffing. Such a model tends to produce a rather thick scrape-off layer: neutrals launched from the walls would generally become ionized in it, leading to an ion density profile with a local maximum in the boundary layer. This effect can be suppressed in the calculations by either using an ad-hoc inward drift term, or - as has been done in the present calculations - by launching the neutrals from a fictitious limiter radius. This, owing to deeper penetration, assures a flat density profile without the use of an empirical inward drift term.

With regard to the dominating transport processes ALCATOR-INTOR scaling was used and the following assumptions were made:

$$\chi_e\,[m^2/s] = 5 \times 10^{19}/n_e\,[m^{-3}]$$
$$D_{D,T} = D_{He} = 0.2\,\chi_e \qquad \text{for } r < r_{sc},$$

$$\chi_e = 1.5$$
$$D_{D,T} = D_{He} = 1.0 \quad [m^2/s] \qquad \text{for } r > r_{sc},$$

where r_{sc} denotes the inner radius of the scrape-off layer. The ion thermal conductivity χ_i was set equal to 3 times the simplified neoclassical value. In the case of helium, an inward diffusion term was also activated. The alpha particle heating model included particle thermalization where the particles are deposited with allowance for first orbit losses.

It should be noted here that the quantitative results of scenario calculation may critically depend upon the transport scaling used (see, for example, /6/). No attempt was made in the present work to investigate the effect of the different scalings available. It is not expected that the basic characteristics of the changes caused by pellets in the recipient discharges, which are associated with deep fuel penetration (as compared with gas puffing), would quantitatively change if slightly different scaling laws were used.

According to an INTOR start-up scenario, a discharge is first heated ohmically ($\Delta\tau_{OH}$ = 3 s) and then by injection of neutral deuterium particles with energy E_{D^0} = 175 keV and total beam current 0.634 kA. The duration of the NB pulse is 6 s. The specified beam current fractions associated with the 1/1, 1/2, and 1/3 energy components are 0.42, 0.38, and 0.20, respectively, and correspond to ion species ratios of $f_{D^+} : f_{D_2^+} : f_{D_3^+}$ = 80 : 15 : 5. The total beam power fed into the plasma is ~ 75 MW. The reference state parameters of an ignited steady-state INTOR discharge are as follows: $\langle n_i \rangle \sim 1.5 \times 10^{20}$ m^{-3}, $\langle T_i \rangle \sim$ 10 to 12 keV, i.e. $\beta_T \sim 5$ %. The maximum value of beta is regulated by a "soft beta limit" built into the code: the electron thermal conductivity is increased everywhere exponentially with increasing β_{pol}: $\chi_e = \chi_{eo} \cdot 1/2 \cdot \exp[\text{ const } \cdot \langle \beta_{pol} \rangle^2]$. In this way the maximum value of β_{tor} is limited to ~ 5 % and the alpha power produced to $P_\alpha \sim$ 130 MW. This set of data was used in continuous fuelling scenario calculations.

In scenario runs pertaining to ignition by density ramp-up, the possibility of reducing the beam energy by suitable matching of the beam and pellet injection parameters was explored. Accordingly, three beam energies were considered: 120 keV, 100 keV, and 80 keV at increased value of the total beam currents. The total beam power fed to the plasma was about ~ 110 MW in these cases at reduced (compared with the standard NB pulse) pulse durations. The beam power was increased because of the enhanced energy losses expected at the lower start-up densities in connection with the ALC.-INT. transport scaling law used. The ion species ratios assumed in these runs are

somewhat different from the INTOR standard and are typical of well-developed ion sources /10/: $f_{D+} : f_{D2+} : f_{D3+} = 85 : 10 : 5$. The resulting current fractions and the respective total particle currents fed to the plasma are shown in Table 1.

E_{D° (keV)	80	100	120	175*
$f_I(E_o)$	0.64	0.62	0.47	0.42
$f_I(E_o/2)$	0.20	0.21	0.28	0.38
$f_I(E_o/3)$	0.16	0.17	0.25	0.20
I (kA)	1.25	1.40	1.75	0.63

Table 1: D° NB heating pulse options considered
*: INTOR reference.

3. Ablation Model and Pellet Data

In most scenario runs, the neutral gas shielding ablation model originally proposed by Parks, Turnbull, and Foster /11/ has been used. This ablation model is based on the assumption of spherical expansion of the ablated material in a (linear or toroidal) magnetic field and does not take into account the effect of a possible pile-up of the low-temperature ionized ablatant in the magnetic flux tubes surrounding the pellet. The semi-empirical expression derived in these analyses for the ablation rate is of the form

$$\dot{N}_{neutr} \propto r_p^{4/3} n_e^{1/3} T_e^{1.64}$$

In some scenario calculations, an optimistic ad hoc assumption regarding the reduction of the ablation rate in a magnetic field has been used: (see Pts I and V of Ref. /5/): $\dot{N}_{magn} = (1.2/T_e) * \dot{N}_{neutr}$, T_e in keV.

The assumption is based on experimental observations /12/ and on earlier analytical and recent numerical calculations /13, 14/, which indicate that the magnetic confinement of the ionized ablatant may cause notable deviations from the ablation rates predicted by the neutral gas shielding ablation model. It should be noted that it is not intended to propose a new ablation model here: $\dot{N}_{magn}$ is merely an assumption aimed at the investigation of the consequences of possible deeper pellet penetration.

The number densities of condensed deuterium and tritium at T ~ 10°K are $n_{D2} \simeq 3.05 \times 10^{28}$ m^{-3} and $n_{T2} \simeq 3.23 \times 10^{28}$ m^{-3}, respectively/15/. Hence a pellet with a radius of approximately $r_p \simeq 0.55$ cm would double the mean density in a standard INTOR discharge ($V \simeq 207.81$ m^3). A 10 % increase of the mean density corresponds to a pellet radius of $r_p \simeq 0.25$ cm. Tritium pellets with a radius of 0.34 cm to 0.37 cm were used for density ramp-up, and deuterium and tritium pellets (alternatingly) with a radius of 0.26 cm to 0.42 cm for repetitive (quasi-continuous) fuelling purposes. The pellet velocity range considered (BALDUR input data) was 2000 m/s to 4000 m/s in the case of repetitive fuelling and a single velocity value of 3000 m/s in the case of density ramp-up.
Note that, because of one-dimensionality, BALDUR neglects vertical plasma elongation and works with an effective radius value $r_{eff} = (r_a \cdot r_b)^{1/2}$. Hence if pellets are injected into the torus in the meridional plane, the velocity required for a certain penetration depth is reduced by a factor $(b/a)^{1/2} \simeq 1.26$ compared with the input data values given above.

4. Ignition by Density Ramp-up

A possible application of pellet injection is ignition of fusion plasmas by a sudden increase of the plasma density. The plasma is first heated at low densities to sufficiently high temperatures, and when the energy stored in the plasma is sufficiently large, a pellet is injected into the discharge, thus stepping up

its density to values necessary to initiate ignition.
Density ramp-up may also be accomplished by a string of pellets, provided the duration of density step-up is shorter than the characteristic energy confinement time. It is assumed that the density increase associated with pellet injection is a nearly adiabatic process. (According to some experimental results /4/, this assumption may not always hold.)
Besides the lower total energy required for heating a low-density plasma (leaving scaling law effects for the moment out of consideration), the heating process is more efficient here: in NB-heated low-density plasmas the energy is preferentially coupled into the plasma ions ("hot ion mode"), which allows enhanced alpha reactions in the heat deposition zone and an early local transition from driven to thermal fusion.

The threshold, i.e. minimum, values of the plasma energy and plasma density, β_{tor} and $\langle n_e \rangle$, required for ignition under the discharge conditions specified in Sec. 2 were determined by taking an ignited INTOR discharge with the standard NB pulse (175 keV/0.634 kA/6 s) and reducing, step by step, the pulse duration until marginal ignition was obtained. This was the case with $\Delta\tilde{\tau}_b \simeq 4$ s. The threshold values of β_T and $\langle n_e \rangle$ were found to be $\beta_T \sim 2.5$ and $n_e \approx 10^{20}$ m^{-3}, respectively (see Figure 1). It should be noted that the soft beta limit option was turned off in the ignition scenario calculations. Note that the β_T and $\langle n_e \rangle$ values thus found do not necessarily corresponds to values associated with optimized heating paths.

All ignition simulation runs were started with an ohmically heated, almost pure tritium discharge ($D^+ : T^+ = 95:5$) maintained at constant density until the start of the NB pulse (t = 3 s) : $\langle n_e \rangle = 4 \times 10^{19}$ m^{-3} for the E° = 120 keV and 100 keV cases, and $\langle n_e \rangle = 1 \times 10^{19}$ for the E° = 80 keV case (feed-back regulation, i.e. gas puffing). The initial plasma density was selected in such a manner as to ensure complete beam penetration at the pulse start with tolerable (< 10 %) shine-through losses. At t = 3 s one of the NB heat pulse options specified in Table 1 was turned on and

kept active until the threshold ignition beta value $\beta_T \sim 2.5$ was reached. Owing to the intense deuterium particle currents associated with the reduced beam energies, the plasma density notably increases during NB injection and becomes rather tritium lean. It was thus found necessary to ramp up the density solely by T_2 pellets (and still be on the tritium-lean side after pellet injection). Hence shortly before the cut-off moment of the NB pulse (~ 10 ms) a T_2 pellet is injected into the discharge, whose mass is selected in such a way as to raise the average density from its momentary value to the required ignition threshold density $\sim 10^{20}$ m^{-3}. The NB pulse data and the resulting pulse durations and pellet sizes required for density ramp-up and ignition are given in Table 2 for the three beam pulse options considered.

Nominal beam energy E_{D° (keV)	175*	120	100	80
Total beam current I (kA)	0.63	1.25	1.40	1.70
Beam pulse length required for ignition $\Delta\tau_B$ (s)	6	2.16	2.68	3.00
T_2 pellet radius required for density ramp-up (cm)	-	0.37	0.34	0.29 (x2)
Pellet injection time (relative NB pulse start) (s)	-	2.15	2.67	1 and 2.99

Table 2: Results of ignition scenario calculations corresponding to $v_{p\ real}$ = 2400 m/s (BALDUR input: v_p = 3000 m/s).

*INTOR reference (with gas-puffing).

Note the decreasing pellet sizes and increasing beam pulse lengths corresponding to increasing total beam particle currents. The total energy fed into the plasma $P_B \cdot \Delta\tau_B$ for obtaining marginal ignition first decreases then increases with decreasing nominal beam energy. In the case of the 80 keV beam option, the beam current is rather intense and the central part of the discharge rapidly becomes tritium-lean. A single T_2 pellet injected at the pulse end is not sufficient

in this case to bring a sufficient amount of fresh fuel to the reaction zone before the temperature starts to decay here, and it was necessary to inject an auxiliary pellet into the discharge 2 s before the end of the beam pulse. Density ramp-up with a single pellet would have required higher pellet velocities in this case.

For each of the beam options considered, reference scenarios with density ramp-up solely by gas puffing have also been computed. Numerous test runs have shown that optimum results correspond in these cases to gas puff durations that are approximately equal to and coincide with the NB pulse durations. Shorter and intenser gas puffs have been tested as well. The corresponding results show that, if the gas puff is triggered at the beginning of the NB pulse, the NB particles are intercepted at the plasma periphery and the central plasma region is cut off from the heat supply, thus impairing ignition. If the gas puff is triggered close to the pulse end, the time required for transporting the fresh fuel from the plasma periphery to the reaction zone by diffusion may be longer than the decay time of the central temperature after the heat pulse has been turned off, and no ignition can be reached. For identical NB heating pulses and for the same initial and final average density values, the reference runs in which pellet injection was replaced with "optimum" gas puffs did not yield ignition.

It may be of interest to note that an 80 keV/1.7 kA/4 s NB pulse combined with density ramp-up by gas puffing yielded ignition, whereas an 80 keV/1.7 kA/5 s NB pulse did not ($\Delta\tau_{g.p.} = \Delta\tau_{B}$). In both cases, the density was increased simultaneously with the NB pulse to the same final value. Hence in the case of the shorter pulse the tritium influx rate is higher, thus resulting in faster inward diffusion. A sufficient amount of fresh fuel could reach the reaction zone before the temperature started to decrease there. In the case of the longer pulse no ignition could be reached, although more energy was fed to the plasma.

Figures 2 and 3 show temperature and density distributions prior to and immediately after pellet injection for the 120 keV beam option.

The time variations of T_e, T_i, n_e, and ß are shown for this case in Figs. 4 and 5, respectively. The corresponding reference scenario (density ramp-up by gas puffing) is illustrated by Figs. 6 and 7, respectively (Fig. 6 shows distributions at the end of the ramp-up pulse). An analysis of these figures shows the basic differences between density ramp-up scenarios obtained with pellet and with gas puffing. Starting with identical initial densities, if the gas puff is actuated simultaneously with an NB pulse, the density and temperature profiles become flattened during the pulse because, as time goes on, the beam is intercepted increasingly further outward. In the case of pellet injection, the density is increased during the NB pulse only by the beam particles themselves, and deep beam penetration with central heating may be maintained up to the moment of pellet injection. Hence the 'hot ion mode' supplemented with centrally peaked density and temperature profiles prevails up to the moment of density ramp-up.

The time variations of T_e, T_i, n_e, and ß shown in Figs. 8 to 11 and in Figs. 12 to 15 correspond to the 100 keV/1.4 kA/2.68 s and 80 keV/1.7 kA/3.0 s beam options, respectively. Note the two pellet injected into the plasma in the 80 keV case. The "reference" cases (Figs. 11 and 15) correspond to density ramp-up by gas puffing.

The sudden temperature drop associated with the injection of a single large pellet into the plasma (the density ramp-up shown in Fig. 3 is accompanied by a $\sim$ 50 % decrease of the average ion temperature) may be "softened up" by replacing the large pellet by a string of smaller pellets within a single energy confinement time. In a test run 9 smaller pellets were injected within 1.3 s into the discharge and ignition was obtained without causing sudded changes in the temperature evolution. Figure 16 shows the temporal variations of n_e, T_e, and $ß_T$ corresponding to this case.

Additional information pertaining to the density ramp-up scenarios is provided in Tables 3 to 5 for the three NB options considered. The values of various plasma parameters ($T_i(o)$, $\langle T_i \rangle$, $\langle n_e \rangle$, β_T, Γ_{div}, $\hat{\tau}_E$, and P_α) are tabulated for three time levels:

(a) The time instant 0.5 s after the start of the NB pulse,
(b) the time immediately after density density ramp-up, and
(c) a time sufficiently long after the density ramp-up.

The reference values shown correspond to density ramp-up by gas puffing. A comparison of the ion temperatures or alpha power outputs (pellet injection vs. reference case) shows appreciable differences for the two methods considered. A comparison of the values corresponding to the second and third time levels indicates the presence or absence of self-substained burning, i.e. ignition. Note that the particle flux into the divertor Γ_{div} immediately after density ramp-up is notably smaller in the case of pellet injection than in the case of gas puffing. This is due to the massive transient flow induced by gas puffing in the outer plasma layers if density ramp-up by means of gas puffing is applied.

Note that the $\sim$ 110 MW beam power applied at reduced beam energies (because of the reduced energy confinement associated with the low start-up densities and the assumed confinement scaling law) might be reduced by increasing, at the same time, the pulse lengths specified in Table 2. No optimization has been done in this respect. A scaling law other than the (1/n)-type here used may further relax the NB heat input requirements.

Table 3 : Density ramp-up scenario data for the 120 keV / 1.25 kA / 2.16 s NB heating pulse case.
Pellet data (T_2): r_p = 0.37 cm, N_p/N_{pla} = 1.05, $V_{p\ real}$ = 2400 m/s, $t_{pel\ inj}$ = 5.15 s.
NB pulse timing: t_{on} = 3.00 s, t_{off} = 5.16 s.
Reference run (density ramp-up with gas puff alone) : LLL 238
Run No. with pellet injection: LLL 624
LLL 620
LLL 210

	t = 3.5 s		t = 5.17 s		t = 11. s	
	Ref. case	Pellet case	Ref. case	Pellet case	Ref. case	Pellet case
$T_i(o)$ [keV]	12.3	13,4	24.2	33.9	25.5	52.0
$\langle T_i \rangle$ [keV]	5.5	6.9	10.0	10.3	7.8	17.4
$\langle T_e \rangle$ [keV]	4.2	4.9	8.0	6.5	6.8	12.9
$\langle n_e \rangle$ [$10^{19} m^{-3}$]	5.1	4.3	9.0	9.9	9.2	9.1
$\langle \beta_T \rangle$ [%]	0.8	0.8	2.4	2.5	2.0	4.6
Γ_{div} [$10^{22} m^{-2} s^{-1}$]	1.8	1.2	3.3	1.4	2.0	2.7
τ_E [s] *	1.2	0.9	2.5	4.0	2.4	2.4
P_α [MW]	7.1	7.1	40.	116.	28.	77.

* Values computed for r = 1.22 m under transient state conditions.

Table 4 : Density ramp-up scenario data for the 100 keV / 1,4 kA / 2.68 s NB heating pulse case.
Pellet data (T_2): r_p = 0.34 cm, N_p/N_{pla} = 0.65,
$V_{p\ real}$ = 2400 m/s, $t_{pel\ inj}$ = 5.67 s.
NB pulse timing: t_{on} = 3.00 s, t_{off} = 5.68 s.
Reference run (density ramp-up with gas puff alone) : LLL 237
Run No. with pellet injection: LLL 623
LLL 212

	t = 3.5 s		t = 5.7 s		t = 11.0 s	
	Ref. case	Pellet case	Ref. case	Pellet case	Ref. case	Pellet case
$T_i(o)$ [keV]	11.4	12.9	21.8	28.5	29.6	41.4
$\langle T_i \rangle$ [keV] $\langle T_e \rangle$ -"-	5.5 4.1	6.2 4.6	10.3 8.2	10.9 7.5	9.3 8.0	13.5 11.0
$\langle n_e \rangle$ [$10^{19} m^{-3}$]	5.0	4.3	9.2	9.6	9.1	9.1
$\langle \beta_T \rangle$ [%]	0.74	0.75	2.5	2.6	2.4	3.6
Γ_{div} [$10^{22} m^{-2} s^{-1}$]	1.7	1.2	3.4	1.8	1.2	2.5
τ_E [s] *	1,0	0.9	2.1	3.7	2.4	2.4
P_α [MW]	5.4	5.4	42.	72.	37.	62.

* Values computed for r = 1.22 m under transient state conditions.

Table 5 : Density ramp-up scenario data for the 80 keV / 1.7 kA / 3.0 s NB heating pulse case.
Pellet data (T_2): r_p = 0.22 cm, N_p/N_{pla} = 0.75 - 0.33
$V_{p\ real}$ = 2400 m/s, $t_{pel\ inj}$ = 4 s and 5.99 s ;
NB pulse timing: t_{on} = 3.00 s, t_{off} = 6.0 s .
Reference run (density ramp-up with gas puff alone) : LLL 242
Run No. with pellet injection: LLL 625
LLL 619

	t = 3.5 s		t = 6.04 s		t = 11. s	
	Ref. case	Pellet case	Ref. case	Pellet case	Ref. case	Pellet case
$T_i(o)$ [keV]	19.8	21.8	21.0	24.3	19.7	34.0
$\langle T_i \rangle$ [keV]	9.7	12.7	10.0	10.4	6.2	11.0
$\langle T_e \rangle$ -"-	4.4	4.9	7.7	7.6	5.7	9.3
$\langle n_e \rangle$ [$10^{19} m^{-3}$]	2.6	2.1	9.5	9.95	9.7	9.7
$\langle \beta_T \rangle$ [%]	0.6	0.6	2.4	2.6	1.7	3.1
Γ_{div} [$10^{22} m^{-2} s^{-1}$]	0.9	0.6	3.9	2.5	1.9	2.3
τ_E [s] *	0.5	0.5	3.0	2.7	2.4	2.5
P_α [MW]	2.2	1.9	33.	60.	25.	53.

* Values computed for r = 1.22 m under transient state conditions.

5. Continuous Fuelling by Pellet Injection

A reactor thermal output of 650 MW requires a fusion reaction rate of approximately 2.3×10^{20} s^{-1}. Assuming a fractional burn-up of ~ 5 % (INTOR specification), at least $\sim 10^{22}$ particles /s must be pumped off at this power level in order to assure the necessary helium pumping rate. Hence under steady-state operational conditions, an equal number of fresh fuel atoms must be added to the plasma (per sec) by gas puffing or pellet injection.

In a series of calculations performed for NET, the optimum combinations of pellet sizes, pellet velocities, and pellet frequencies were investigated by injecting a string of 10 pellets, D_2 and T_2, alternatingly, ("continuous" fuelling) into an already ignited standard INTOR plasma. Before and after pellet injection, the density was kept at a constant level by gas puffing. The same transport scaling laws were assumed here as in the case of the ignition scenarios (ALCATOR-INTOR) with an addition: the "soft beta limit" was applied to obtain steady-state burn conditions.

Preliminary results obtained have shown that the response of the recipient discharge to the injection of a continuous string of pellets, i.e. the change of the temperature and density distributions, the onset of favourable or unfavourable profiles and the resulting changes of the particle and energy confinement times are functions of the pellet mass-velocity-frequency combinations applied. Hence, for determining the optimum injection characteristics, systematic scanning of these parameters was performed on the basis of the following considerations: First, deep pellet penetration produces favourable density profiles, improves the confinement time, and increases the alpha production rate. Hence for a given velocity the pellet mass should be large enough to ensure deep penetration and yet small enough not to cause large-amplitude density fluctuations. Second, the pellet frequency required for continuous fuelling depends on the particle confinement time associated with the modulated density and temperature profiles developing during continuous pellet fuelling. Care should be taken that the frequencies chosen and the respective injection periods are different from the characteristic response

time associated with burn control ($\gtrsim$ 1 s). Third, the particle exhaust flux should be large enough to ensure the rate required for helium pump-off.

In the optimization runs, for a given pellet size-pellet velocity combination, the pellet frequency was varied until the time average of the modulated mean plasma became approximately constant.

Representative results of continuous fuelling scenario calculations are shown in Figs. 17 to 28. In each figure, the temporal variations of $T_i(o)$, $\langle T_i \rangle$, $n_e(o)$, $\langle n_e \rangle$, and $n_\alpha(o)$ associated with the repetitive injection of (10) pellets are shown. Figures 17 to 22 correspond to the neutral gas shielding ablation model, while Figs. 23 to 28 to the magnetic shielding approximation used. In both cases, the first three figures were computed with $v_{inj} \approx$ 1600 m/s (2000 m/s BALDUR input) and the last three ones with $v_{inj} \approx$ 3200 m/s (4000 m/s BALDUR input) pellet velocities. Three pellet size/frequency combinations were considered for each velocity: r_p/f_p = 0.26 cm/6.7 Hz, 0.33 cm/3.3 Hz, and 0.42 cm/1.7 Hz, corresponding approximately to the same fuelling rate (3.0 to 3.5 x 10^{22} s^{-1}). Consider now the cases shown in Figs. 18 and 24 (or Figs. 21 and 27) corresponding to the same pellet sizes (0.33 cm/3.3 Hz) and pellet velocities (1200 m/s for Figs. 18 and 24 and 3200 m/s for Figs. 21 and 27) but to different ablation rate approximation.

The effect of deep pellet penetration associated with the magnetic shielding approximation is apparent: the central density changes almost simultaneously with the average density and, owing to the high density and improved energy confinement in the plasma centre, enhanced alpha particle production results there. The corresponding temperature changes indicate

that deeper fuelling is associated with a larger temperature drop in the plasma centre. However, owing to the onset of enhanced alpha heating the central temperature rapidly recovers. The amplitude of the average density modulation, i.e. the $\Delta n_e/\langle n_e \rangle$ ratio is approximately 9 % in this case. Keeping the fuelling rate unaltered, we changed (both increased and decreased) the pellet injection frequency by a factor of 2 (high-frequency cases: Figs. 18, 21, 24, and 27; low-frequency cases: Figs. 20, 23, 26, and 29). One will note the downward drift of the mean density in the high-frequency case. The fuelling rate chosen is apparently not sufficient in this case to compensate the enhanced particle losses associated with the smaller penetration depths of the small pellets. A slight drift of the mean plasma density during pellet injection can be observed in all figures displayed. This drift is due to profile readjustments in the plasma, which may take several seconds under reactor conditions (see the $\langle T_i \rangle$ and particularly the $T_i(o)$ curves). Apparently, a larger number of pellets would be necessary for simulating truly quasi-steady end states.

Some results of the fuelling scenario calculations corresponding to the two different pellet velocities and the two ablation rate approximations considered are summarized in Tables 6 and 7. Some of the quantities appearing in these tables are normalized with respect to values corresponding to gas puffing (subscript g). Note the improved output characteristics associated with deep pellet penetration. However, even with $v_{real} \approx 1600$ m/s and the (pessimistic) neutral gas shielding ablation model an increase of the alpha power output of over 8 % is observed in the case of pellet injection ($\Delta n/\langle n \rangle \sim 9$ %) as compared with gas puffing. Since $P_\alpha \propto \beta_T^2$, a part of the alpha power enhencement is a result of the increased average β_t value, while the rest can be attributed to profile changes produced by pellet injection.

The quantity

$$P_\alpha^* = (P_\alpha / P_{\alpha g}) / (\beta_t / \beta_{tg})^2$$

appearing in Tables 6 and 7 represent normalized alpha power output caused solely by profile changes.

As can be seen, while in the case of the neutral gas shielding ablation model the alpha power production increases with increasing pellet size and/or pellet velocity (see also the variations of β_t and P_α^*), in the case of the magnetic shielding approximation P_α reaches a plateau, or even decreases (P_α^*) with increasing pellet size. The reason for such a behaviour is obvious: while in the first case the pellet penetration depths are still far away from central, in the second case they are rather large and no further improvement of $P_\alpha / P_{\alpha g}$ (or P_α^*) may be expected. Moreover, the massive cooling of the plasma center by the largest pellets applied (r_p = 0.42 cm) inhibits the alpha particle production rate there. Hence care should be exercised in selecting the pellet injection parameters when central fuelling is considered.

The particle flux into the divertor is reduced (typically by 35 %) if pellet injection is applied. However, the particle exhaust fluxes obtained (typically 3.5 x 10^{22} m^{-2} s^{-1}) are still more than sufficient for ensuring the necessary helium pumping rate. It should be noted, however, that the exhaust flux values obtained are functions of the edge model used in the calculations (intense localized recycling in the divertor chamber).

Table 6 : Continuous fuelling at a given particle input rate ($\sim 3 \times 10^{22}$ s^{-1})
Neutral gas shielding ablation model .

Subscript g denotes values corresponding to gas puffing.

Pellet radius r_p (cm) Pellet frequency f_p (s^{-1}) Density perturbation $\Delta n/\langle n \rangle$	0.26 6.7 0.03		0.33 3.3 0.085		0.42 1.7 0.20	
Run No. (LLL)	072	064	073	051	074	061
Pellet velocity (m/s) (BALDUR input value)	2000	4000	2000	4000	2000	4000
Penetration depths of the first two (D_2/T_2) pellets (cm)	42/42	46/51	46/51	56/62	56/62	67/79
Alpha power production $P_\alpha / P_{\alpha g}$ (P^*_α)	1.06 (1.08)	1.11 (1.11)	1.08 (1.06)	1.16 (1.11)	1.17 (1.15)	1.26 (1.21)
Toroidal total beta $\beta_{tor} / \beta_{tor\ g}$	0.99	1.00	1.01	1.02	1.01	1.02
Particle flux into divertor Γ / Γ_g	0.64	0.61	0.64	0.64	0.65	0.62

Table 7 : Continuous fuelling at a given particle input rate ($\sim 3 \times 10^{22}$ s^{-1})
Ablation model with magnetic shielding approximation .
Subscript g denotes values corresponding to gas puffing.

Pellet radius r_p (cm) Pellet frequency f_p (s^{-1}) Density perturbation $\Delta n/\langle n \rangle$	0.26 6.7 0.03		0.33 3.3 0.085		0.42 1.7 0.20	
Run No. (LLL)	071	067	070	056	069	068
Pellet velocity (m/s) (BALDUR input value)	2000	4000	2000	4000	2000	4000
Penetration depths of the first two (D_2/T_2) pellets (cm)	67/73	90/96	79/90	113/125	102/113	142/165
Alpha power production $P_\alpha / P_{\alpha g}$ (P^*_α)	1.16 (1.16)	1.34 (1.29)	1.32 (1.15)	1.38 (1.23)	1.30 (1.16)	1.27 (1.20)
Toroidal total beta $\beta_{tor} / \beta_{tor\,g}$	1.00	1.02	1.07	1.06	1.06	1.03
Particle flux into divertor Γ / Γ_g	0.63	0.62	0.65	0.63	0.65	0.62

6. Discussion and Conclusions

The results of scenario calculations seem to prove the superiority of pellet injection over other fuelling methods under thermonuclear plasma conditions, in spite of a number of uncertainties inherent in the present calculations. Let us briefly summarize the factors that may affect the accuracy of the results obtained.

(a) Both the transport code and the ablation models used are 1-D approximations, whereas a pellet injected into a plasma means a massive local perturbation of the recipient medium. Hence the problem is truly three-dimensional, and the accuracy associated with the 1-D approaches applied is unknown.

(b) The results of transport code calculations strongly depend upon the transport scaling models used. Should the actual transport processes notably deviate from the ALCATOR-INTOR scaling applied here, some of the conclusions may have to be modified.

(c) The neutral shielding ablation model and its "magnetic" variant applied here are based on the assumption that pellet ablation is caused primarily by thermal electrons present in the plasma. Estimates pertaining to the effect of nonthermal particles such as NB ions, alpha particles and runaway electrons /5/ show that this assumption may not always be true. The actual pellet ablation rate is most likely determined by the simultaneous action of all relevant energy carriers present in the plasma.

(d) There exists experimental evidence according to which pellet ablation may not always be considered as an adiabatic process. In experiments on ASDEX /4/, the energy content of the plasma dropped somewhat every time a pellet was injected. It was shown some time ago that pellets may serve as targets for CX collisions and may thus cause enhenced energy losses /16/.

However, because of the 3-D nature of the problem, it is difficult to estimate quantitatively the magnitude of CX energy losses on the basis of 1-D transport code calculations. The effect of possible MHD activities excited by pellets in the recipient plasma could not be taken into account in the present scenario calculations either.

(e) The scrape-off layer model used in the present calculations (a parallel flow Mach number ~ 0.02 with intense localized recycling in the divertor chamber) may also limit the generalization of the results obtained.

In spite of the uncertainties listed, pellet injection in thermonuclear plasmas seems to possess a number of advantages not matched by any other fuelling method. The principal advantage of the method lies in the reduced transport time of the fresh fuel particles from the plasma boundary to the heat deposition (or alpha reaction) zone. Hence:

1. If ignition is attempted in a NB-heated plasma by density ramp-up, pellet injection makes it possible to start with a plasma density sufficiently low to ensure deep beam penetration, central particle deposition and thus peaked temperature and density profiles. Advantage can be taken of the 'hot ion mode' in this case.

2. Transition from NB-driven fusion to self-substained alpha particle production may be possible at lower beam energies and shorter beam pulses (with increased beam currents) than in the case of gas puffing (see Table 2).

3. Pellet injection transports fresh fuel to the reaction zone on a time scale that is much shorter than the diffusion time characterizing the method with gas puffing. While in the case

of density ramp-up by gas puffing the ramp-up time is finite and the beam may be blocked off at the plasma periphery before the heating pulse is off, density ramp-up by pellet injection is practically instantaneous and unimpaired beam penetration may be granted during the entire heating phase.

5. As regards continuous fuelling, repetitive pellet injection produces peaked density and temperature profiles. It also increases the central β_{tor} values and may cause a substantial increase of the thermal alpha power output over the value predicted with gas puffing (approximately 8 % in the case of the neutral shielding ablation model coupled with shallow pellet penetration, i.e. with $v_{real} \approx 1600$ m/s, and approx. 30 % in the case of magnetic shielding approximation coupled with $v_{real} \approx 3200$ m/s).

6. The particle exhaust flux corresponding to pellet fuelling is somewhat reduced compared with edge fuelling, but is still more than sufficient for effective helium pump-off.

Acknowledgements

This study is part of an analysis performed for NET on the basis of EURATOM Contract No. 138/83-11/NET. Useful discussions with K. Borrass and F. Engelmann of the NET Team, K. Lackner, J. Neuhauser and E. Speth of IPP are gratefully acknowledged.

References

/1/ GREENWALD, M., GWINN, D., MILORA, S., PARKER, J., and PARKER, R., Phys. Rev. Lett., 53 (1984) 352.

/2/ SENGOKU, M., FOSTER, C.A., and STOCKDALE, R., in Plasma Physics and Controlled Nuclear Fusion Research (Proc. 10th Int.Conf., London, 1984), post-deadline paper.

/3/ SCHMIDT, G.L., of PPPL, private communication (1983).

/4/ VLASES, G., KAUFMANN, M., GRUBER, O., HAAS, G., et al., paper presented at the 12th Europ.Conf. on Controlled Fusion and Plasma Physics, Budapest, Sept. 1985, see also GOLDSTON, R.J. (PPPL), informal presentation, Garching (1985).

/5/ LENGYEL, L.L., Assessment of Pellet Injection for the Next European Torus, Pts. I to IV: IPP Repts. 1/231 to 1/233 (1984), and Pt. V: 1/236 (1985).

/6/ WATKINS, M.L., STRINGER, T.E., GIBSON, A., CORE, W.G.F., ROBERTSON, I.L., CORDEY, J.G., and FIELD, J.J., in Plasma Physics and Controlled Nuclear Fusion Research (Proc. 8th Int. Conf., Brussels, 1980), Vol. 1, IAEA, Vienna (1981) 639.

/7/ HOLMES, J.A., ROME, J.A., HOULBERG, W.A., PENG, Y.-K.M., and LYNCH, S.J., Nucl. Fusion 20, (1980) 59.

/8/ HOULBERG, W.A., ATTENBERGER, S.E., and HIVELY, L.M., Nucl. Fusion 22 (1982) 935.

/9/ POST, D.E., SINGER, C.E., MCKENNEY, A.M., Working Draft of the BALDUR Documentation, Princeton PPL, TFTR Physics Group, Rept. No. 33 (1981).

/10/ SPETH, E., (IPP), private communication (1985).

/11/ PARKS, P.B., TURNBULL, R.S., and FOSTER, C.A., Nucl. Fusion 17 (1977) 539; see also MILORA, S.C., and FOSTER, C.A., IEEE Trans. Pla.Sci. 6 (1978), 578, or PARKS, P.N. and TURNBULL, R.J., Phys. Fluids 21 (1978) 1735.

/12/ THOMAS, C.E., An Experimental Investigation of Solid Hydrogen Pellet Ablation in High Temperature Plasmas, ORNL/TM-7486 (1981).

/13/ LENGYEL, L.L., Phys. Fluids 21 (1978) 1945.

/14/ KAUFMANN, M., LACKNER, K., LENGYEL, L.L., and SCHNEIDER, W., paper submitted to Nucl. Fusion; see also Verhandl. DPG (Bull. Germ. Phys. Soc.) VI, 19 (1984), 1210.

/15/ SOUERS, P.C., LLL Rept. UCRL-52226 (1977).

/16/ LENGYEL, L.L., On Pellet-Induced Charge Exchange Effects in Ohmic and NB-Heated Tokamak Plasmas, IPP Rept. 1/213 (1983).

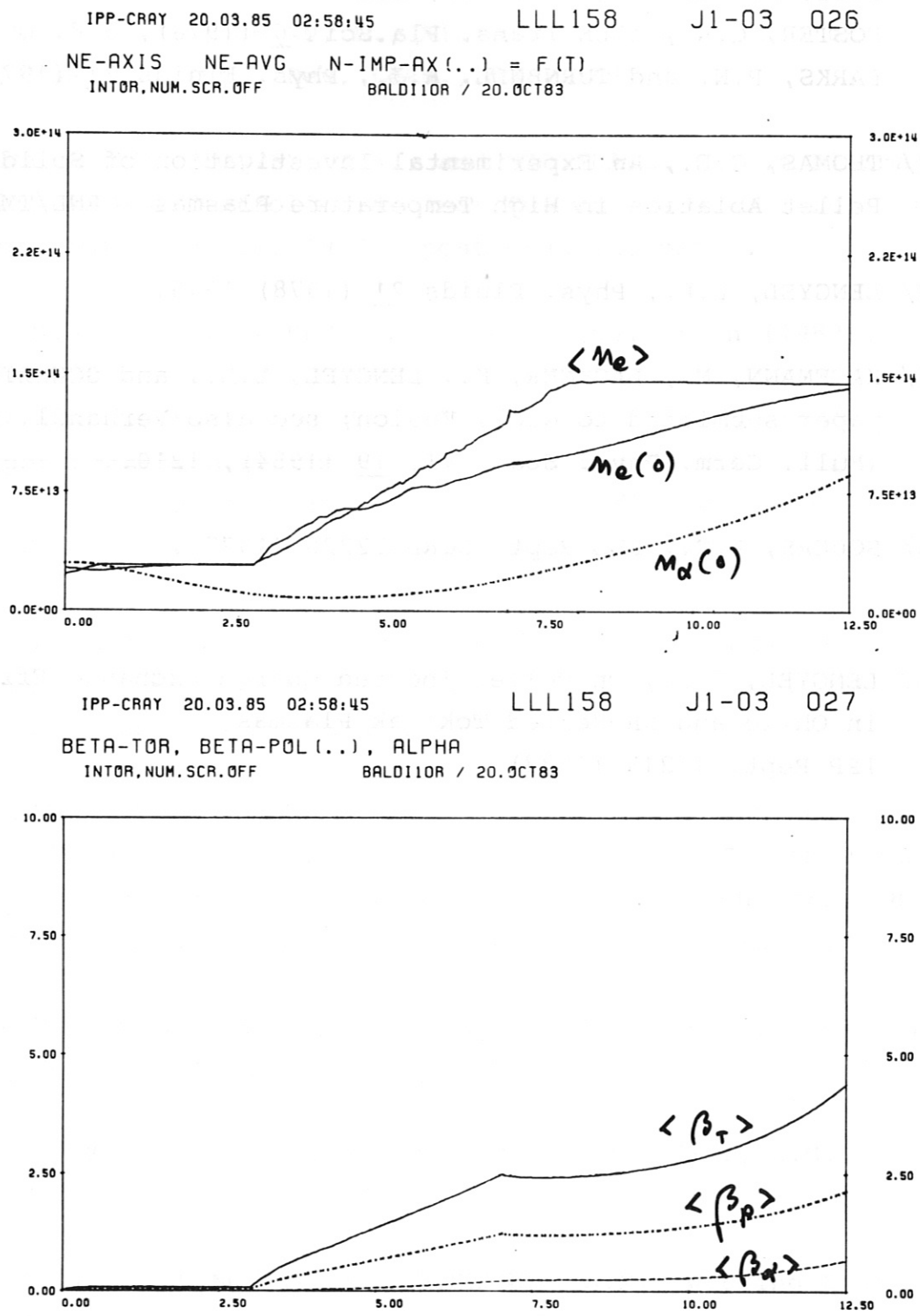

Fig. 1: Determination of the threshold values of $\langle \beta_t \rangle$ and $\langle n_e \rangle$ necessary for ignition in INTOR.

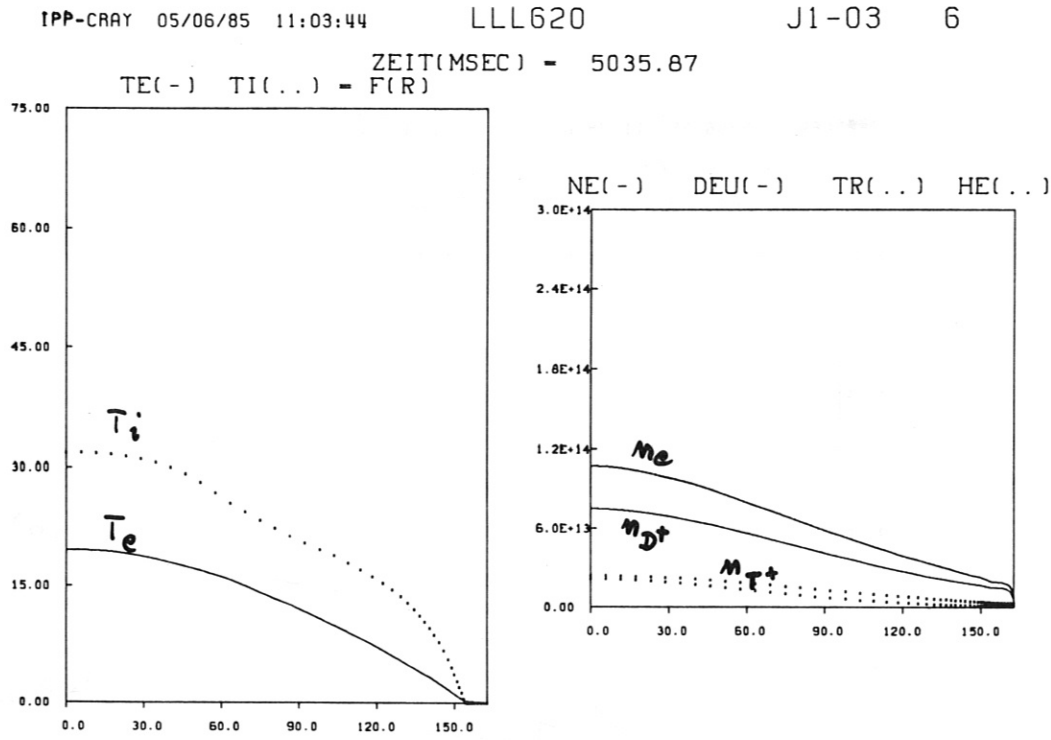

Fig. 2: Radial temperature and density distributions before pellet injection (t_p = 5.15 s) for the 120 keV/1.25 kA/2.16 s NB pulse case.

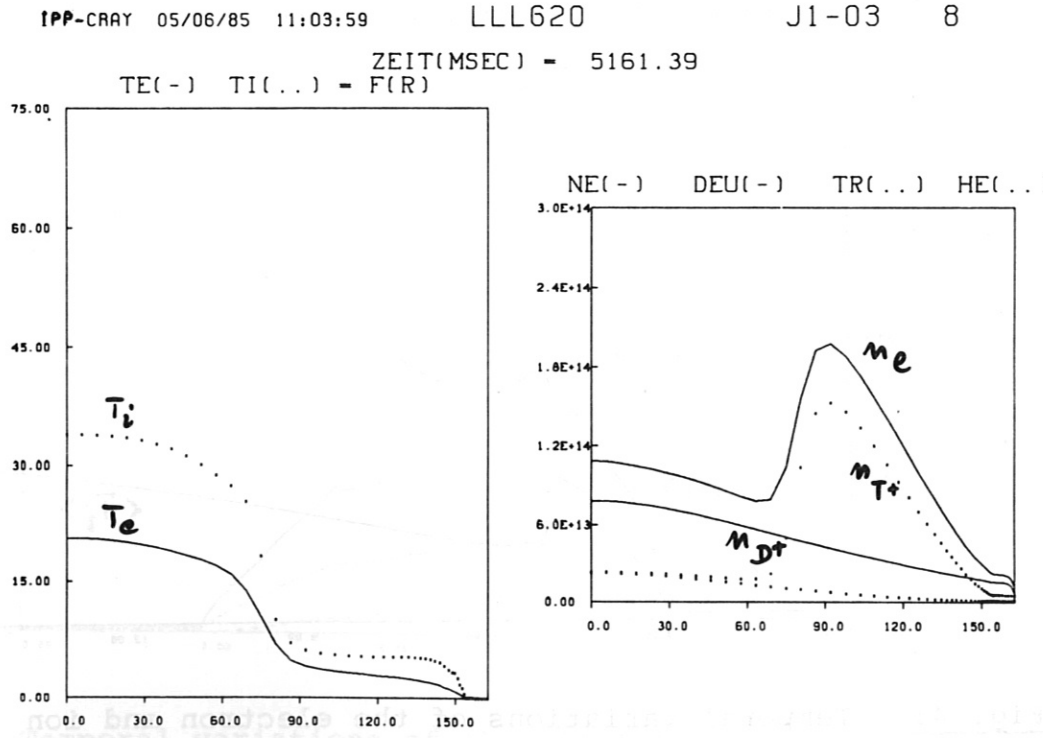

Fig. 3: Radial temperature and density distributions after pellet injection (v_p = 2400 m/s, r_p = 0.37 cm, T_2 pellet) for the 120 keV/1.25 kA/2.16 s NB pulse case.

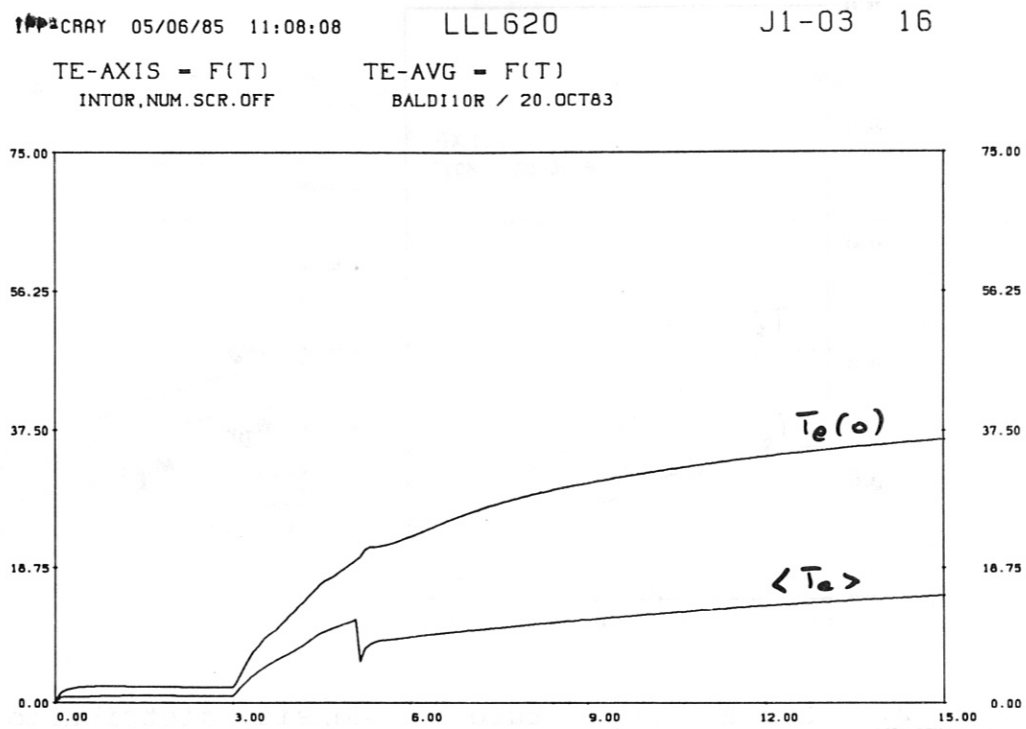

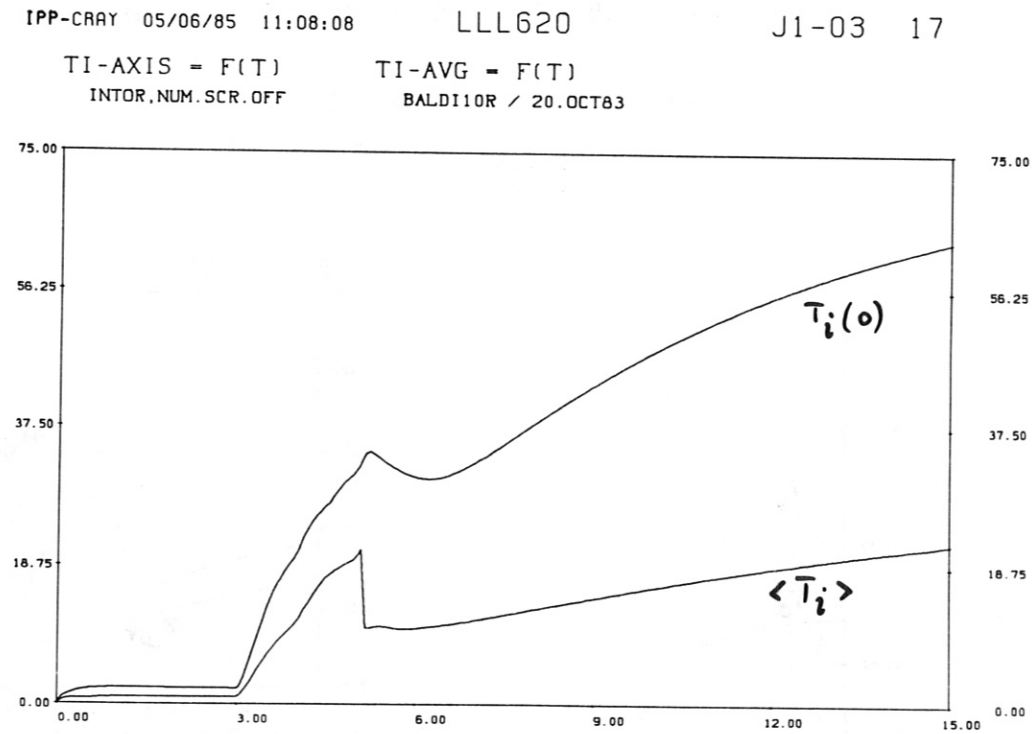

Fig. 4: Temporal variations of the electron and ion temperatures during density ramp-up by pellet injection for the 120 keV/1.25 kA/2.16 s NB pulse case.

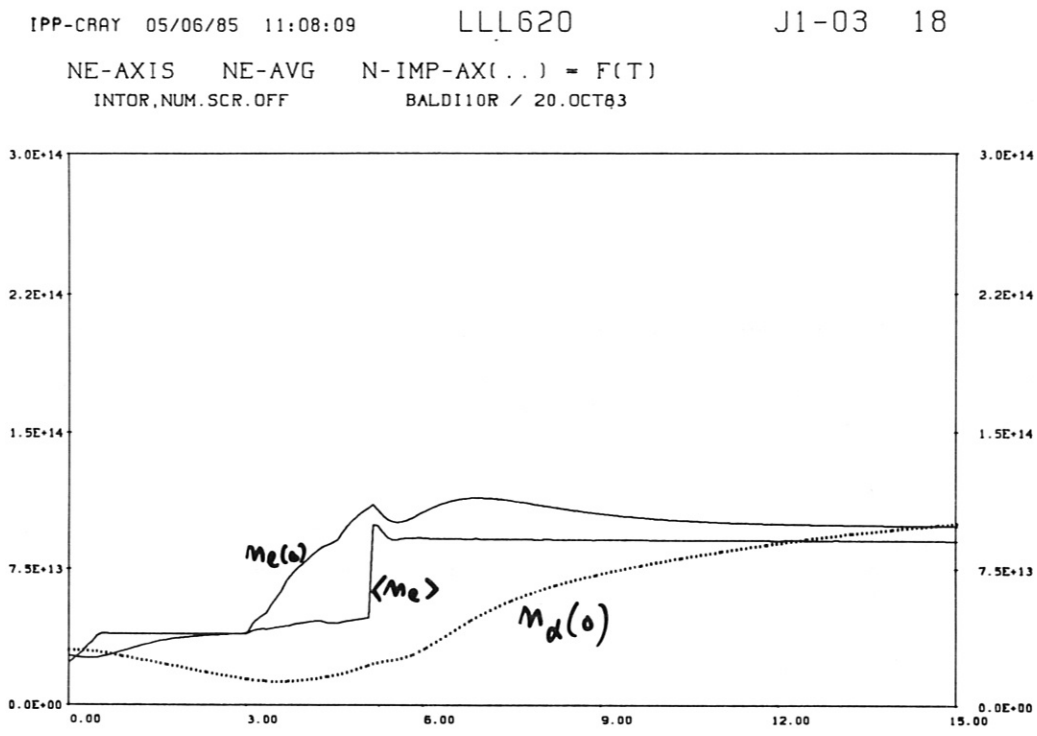

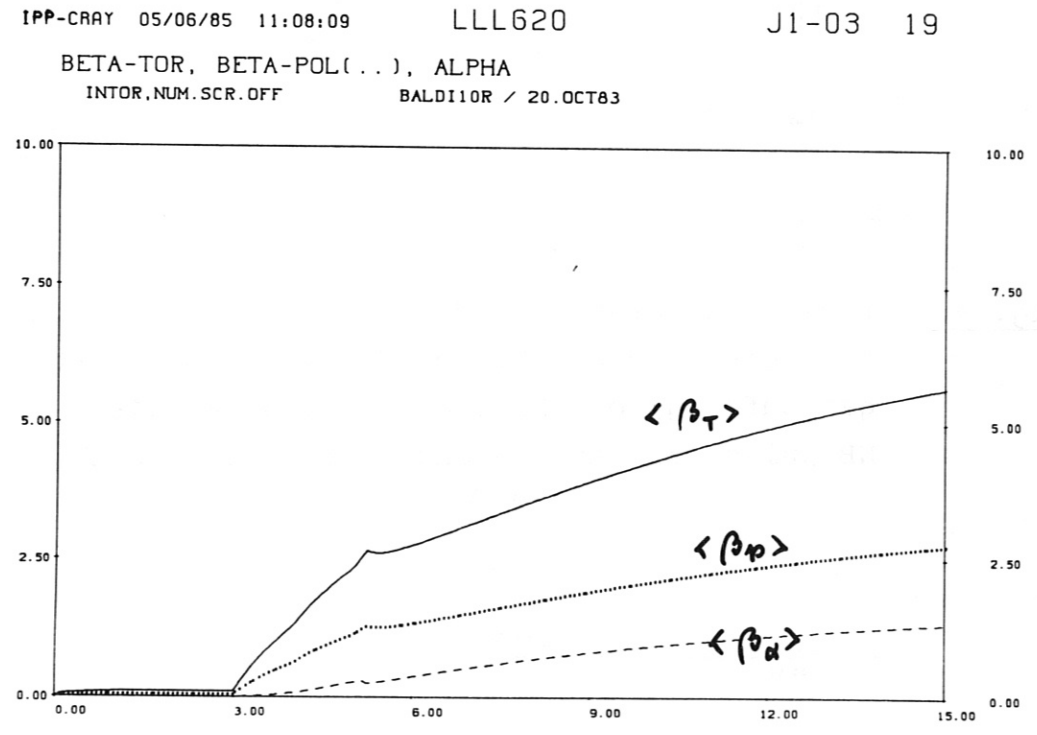

Fig. 5: Temporal variations of the electron and alpha particle densities and of the beta values during density ramp-up by pellet injection for the 120 keV/1.25 kA/2.16 s NB pulse case.

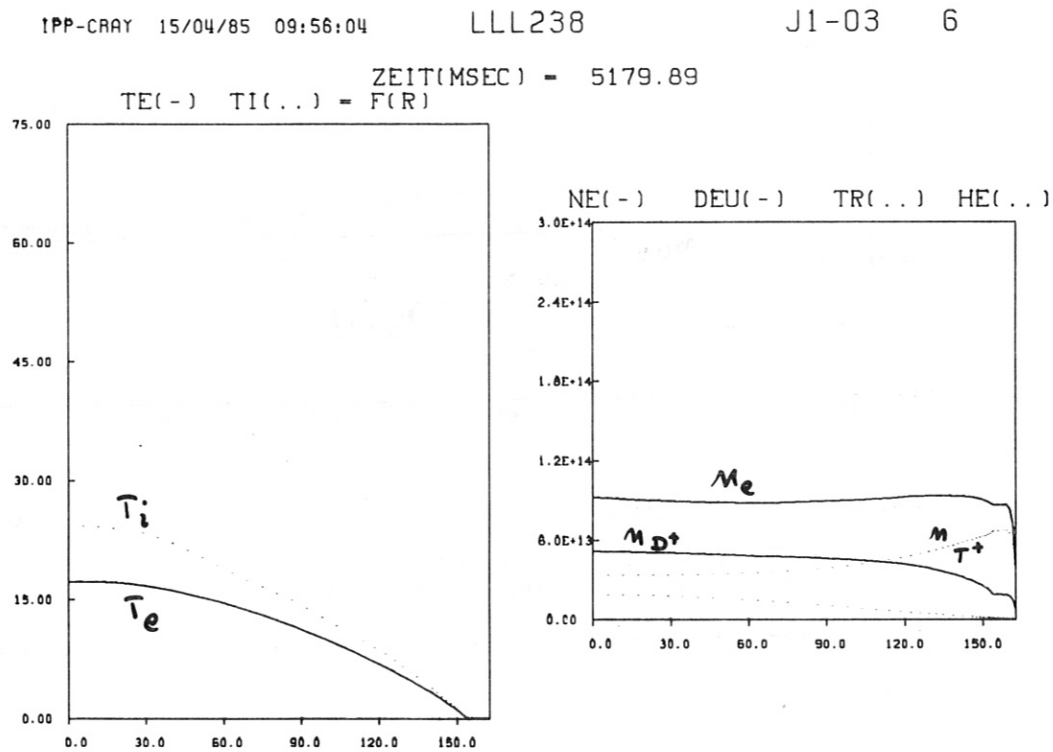

Fig. 6: Radial temperature and density distributions for the reference discharge (density ramp-up by gas puffing) of the 120 keV/1.25 kA/2.16 s NB pulse case at the end of the ramp-up phase.

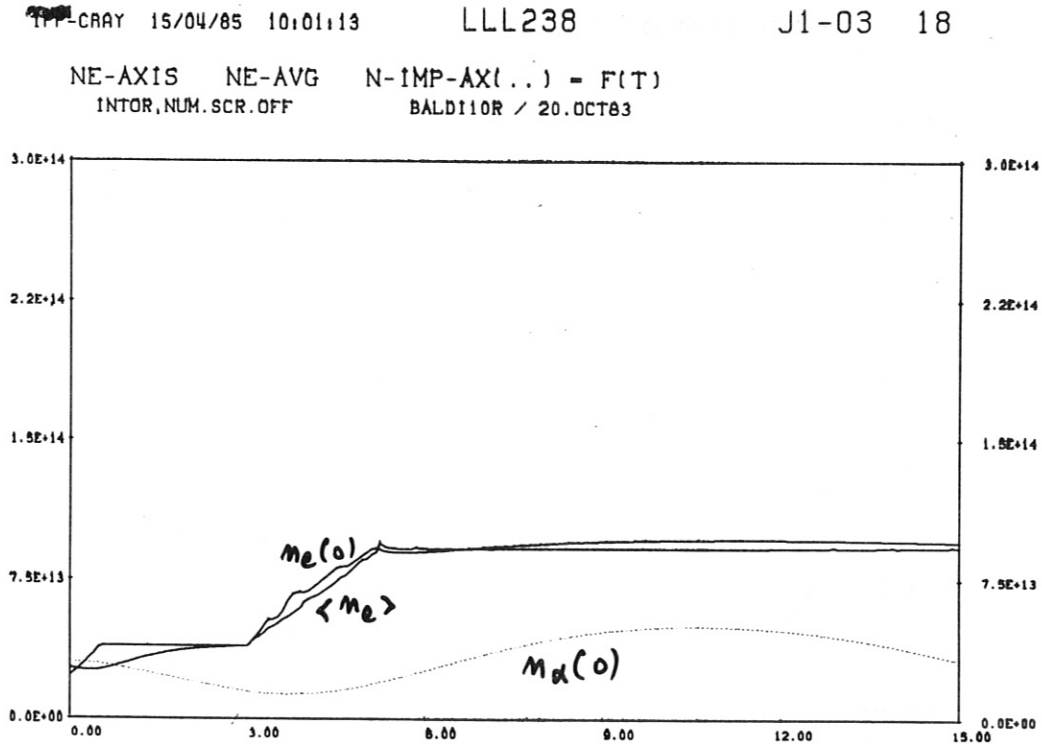

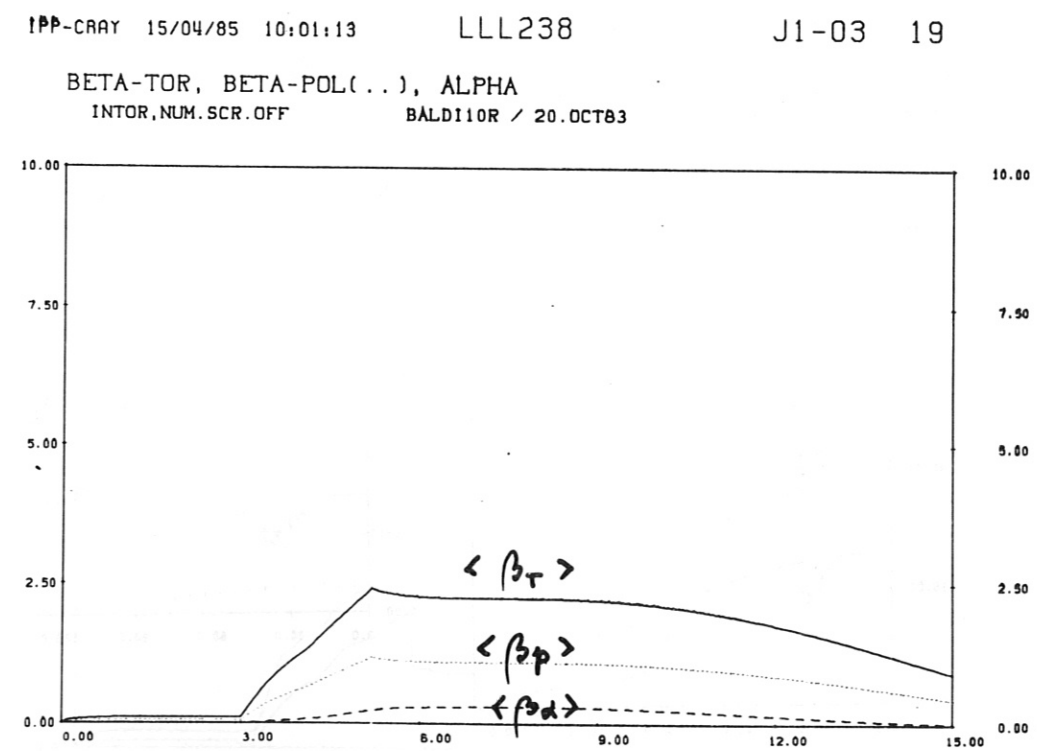

Fig. 7: Temporal variations of the electron and alpha particle densities and of the beta values for the reference discharge (density ramp-up by gas puffing) of the 120 keV/1.25 kA/2.16 s NB pulse case.

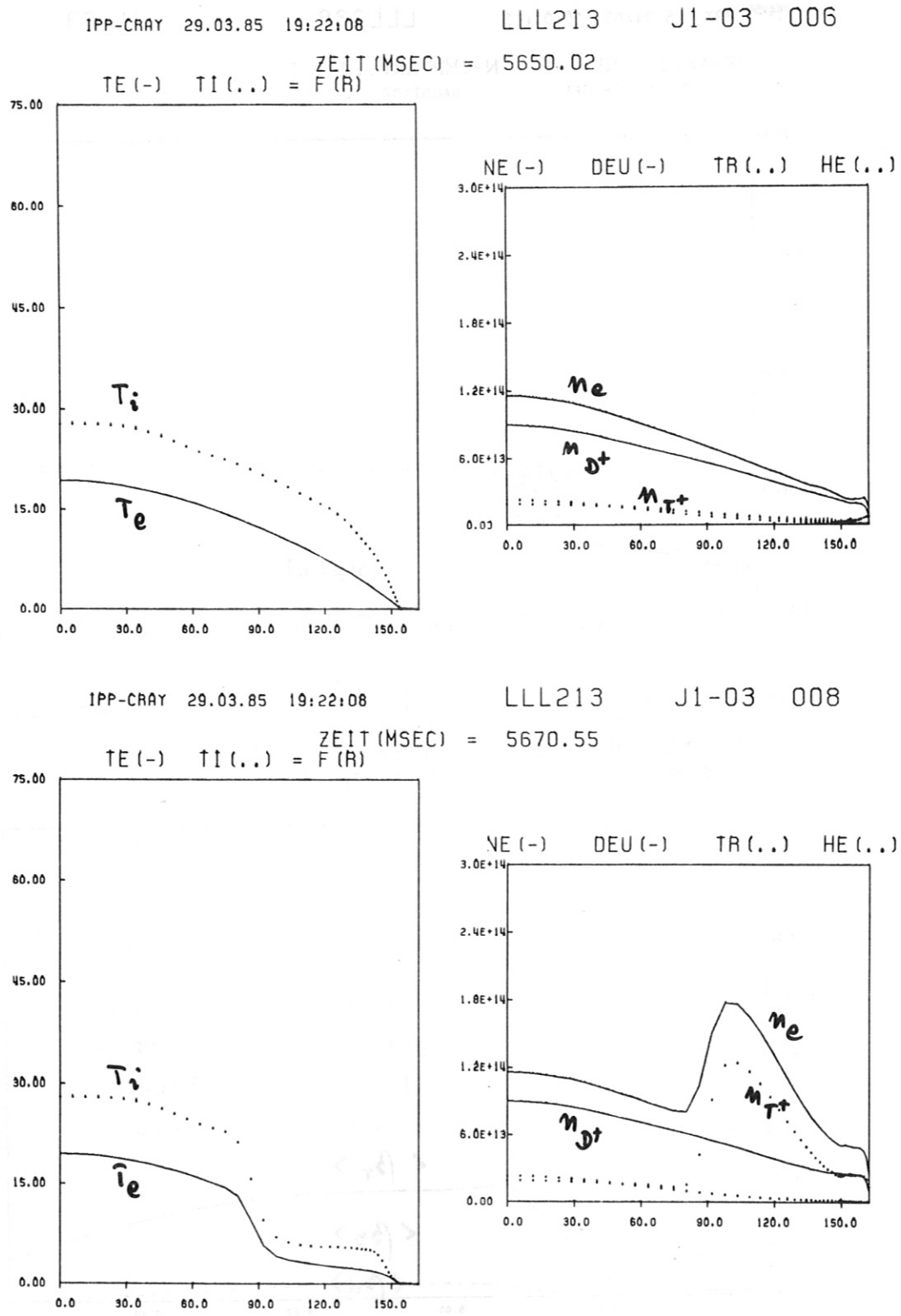

Fig. 8: Radial temperature and density distributions before and after pellet injection (t_p = 5.67 s) for the 100 keV/1.4 kA/2.68 s NB pulse case. Pellet size and velocity: r_p = 0.34 cm, and v_p = 2400 m/s, respectively.

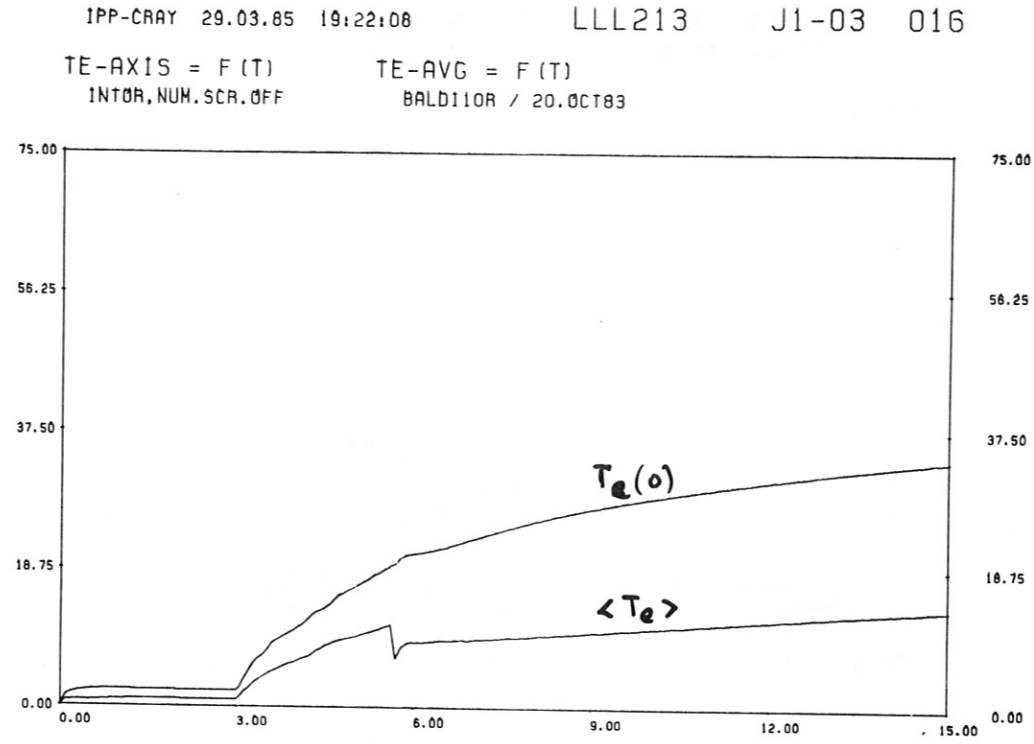

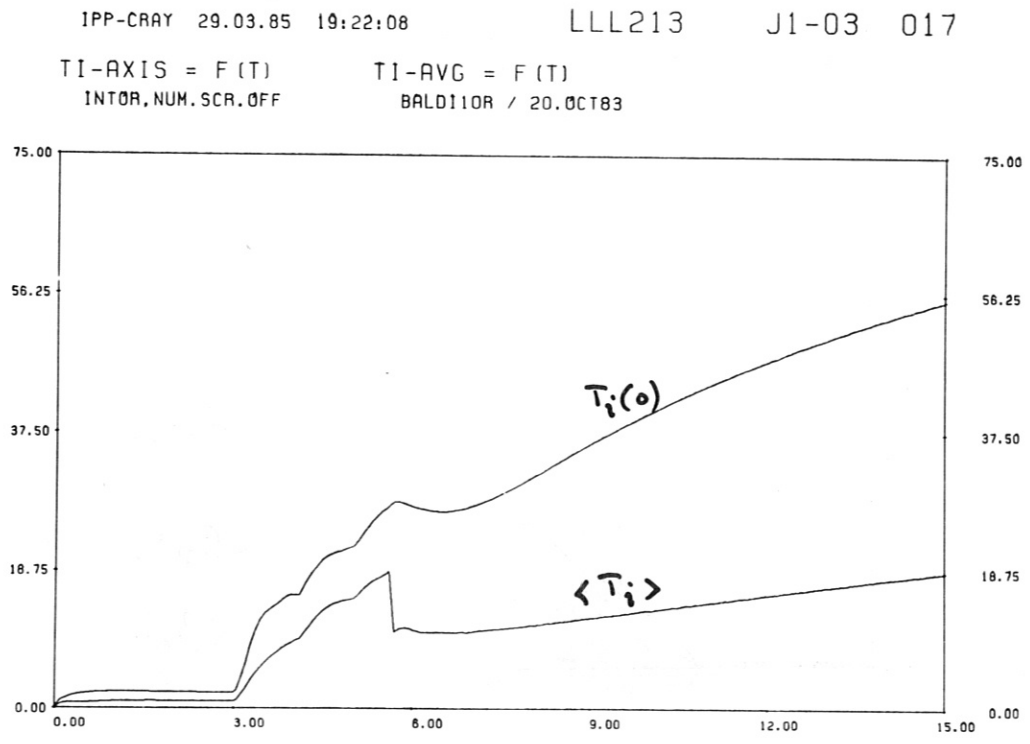

Fig. 9: Temporal variations of the electron and ion temperatures during density ramp-up by pellet injection for the 100 keV/1.4 kA/2.68 s NB pulse case.

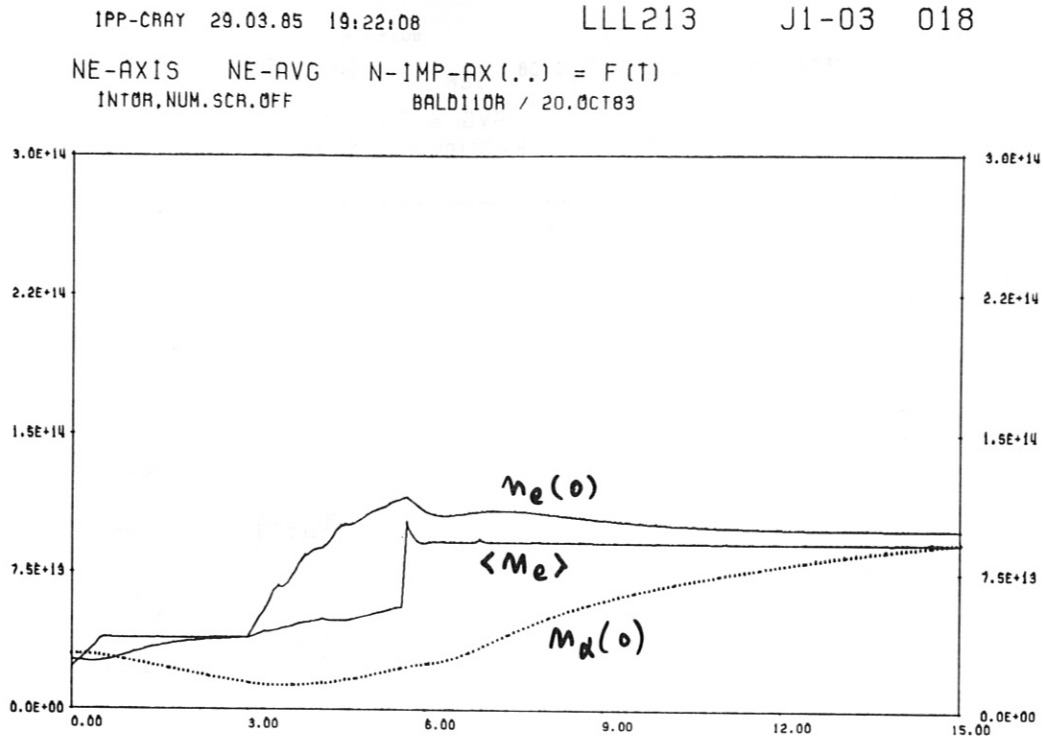

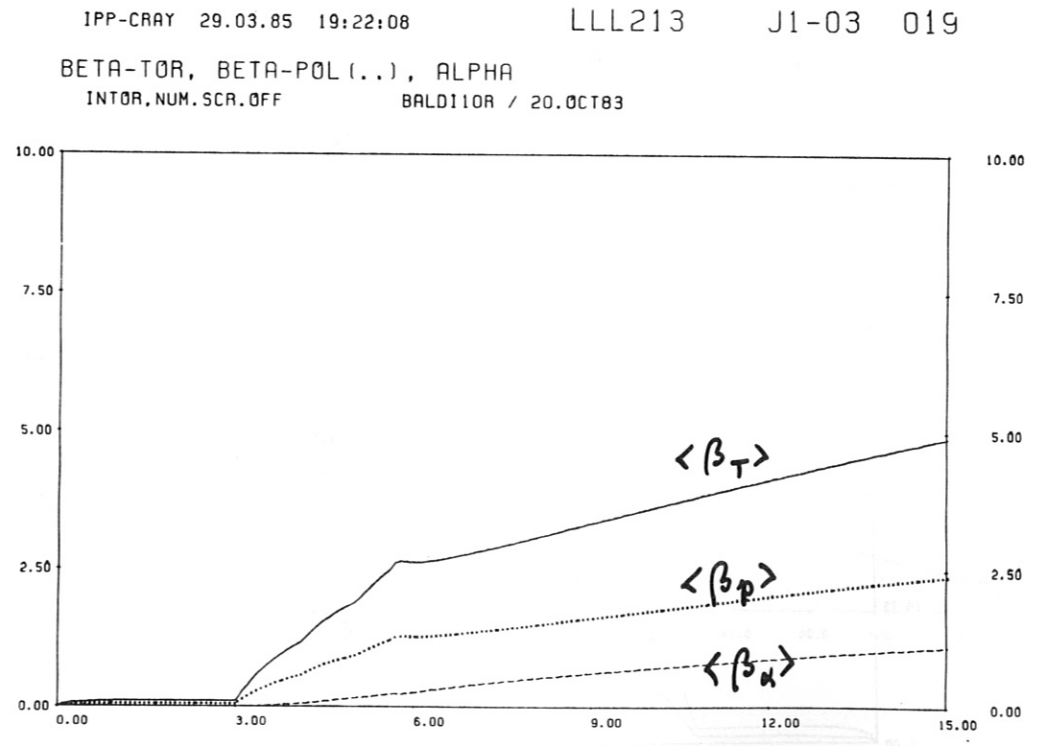

Fig. 10: Temporal variations of the electron and alpha particle densities and of the beta values during density ramp-up by pellet injection for the 100 keV/1.4 kA/2.68 s NB pulse case.

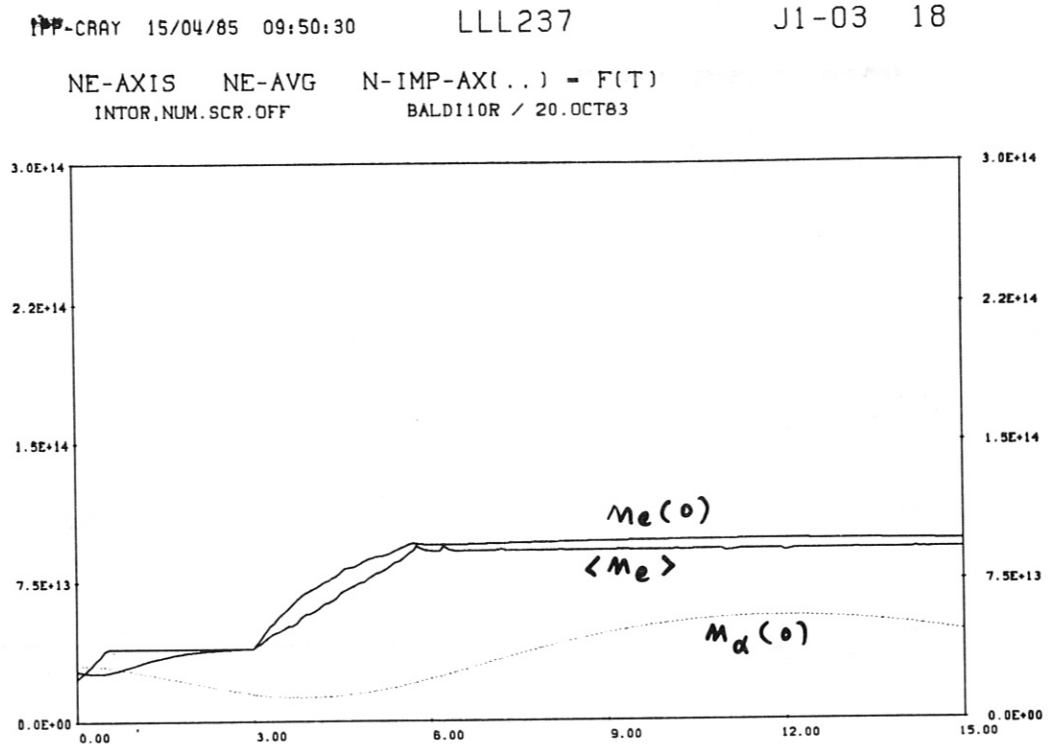

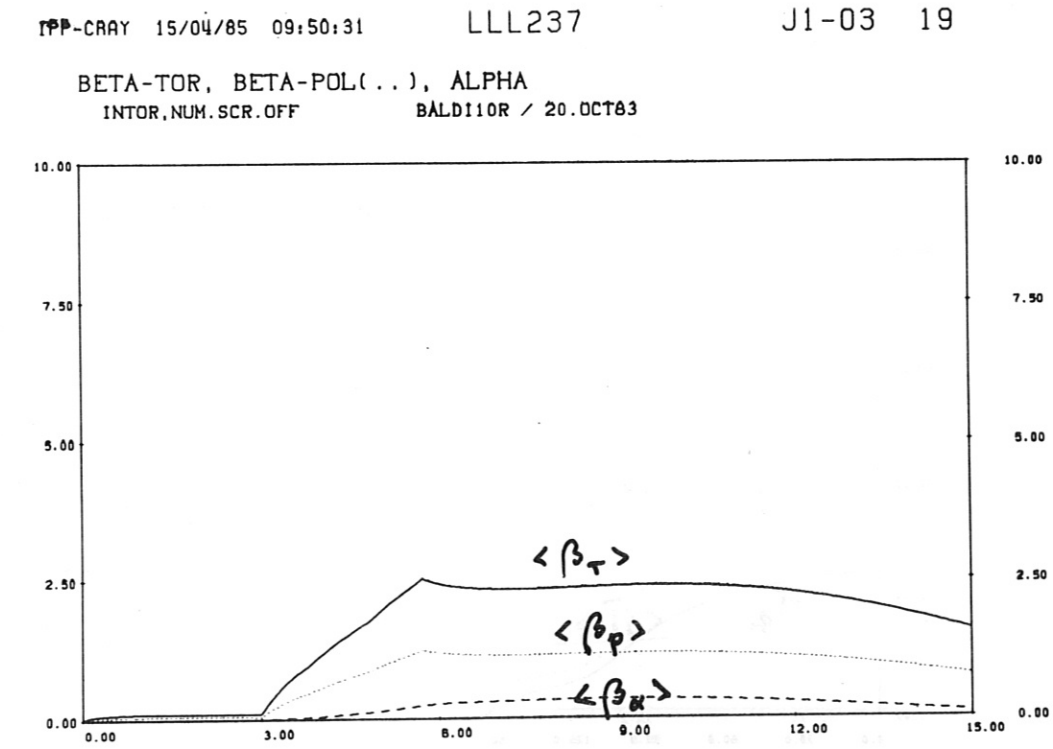

Fig. 11: Temporal variations of the electron and alpha particle densities and of the beta values for the reference discharge (density ramp-up by gas puffing) of the 100 keV/1.4 kA/2.68 s NB pulse case.

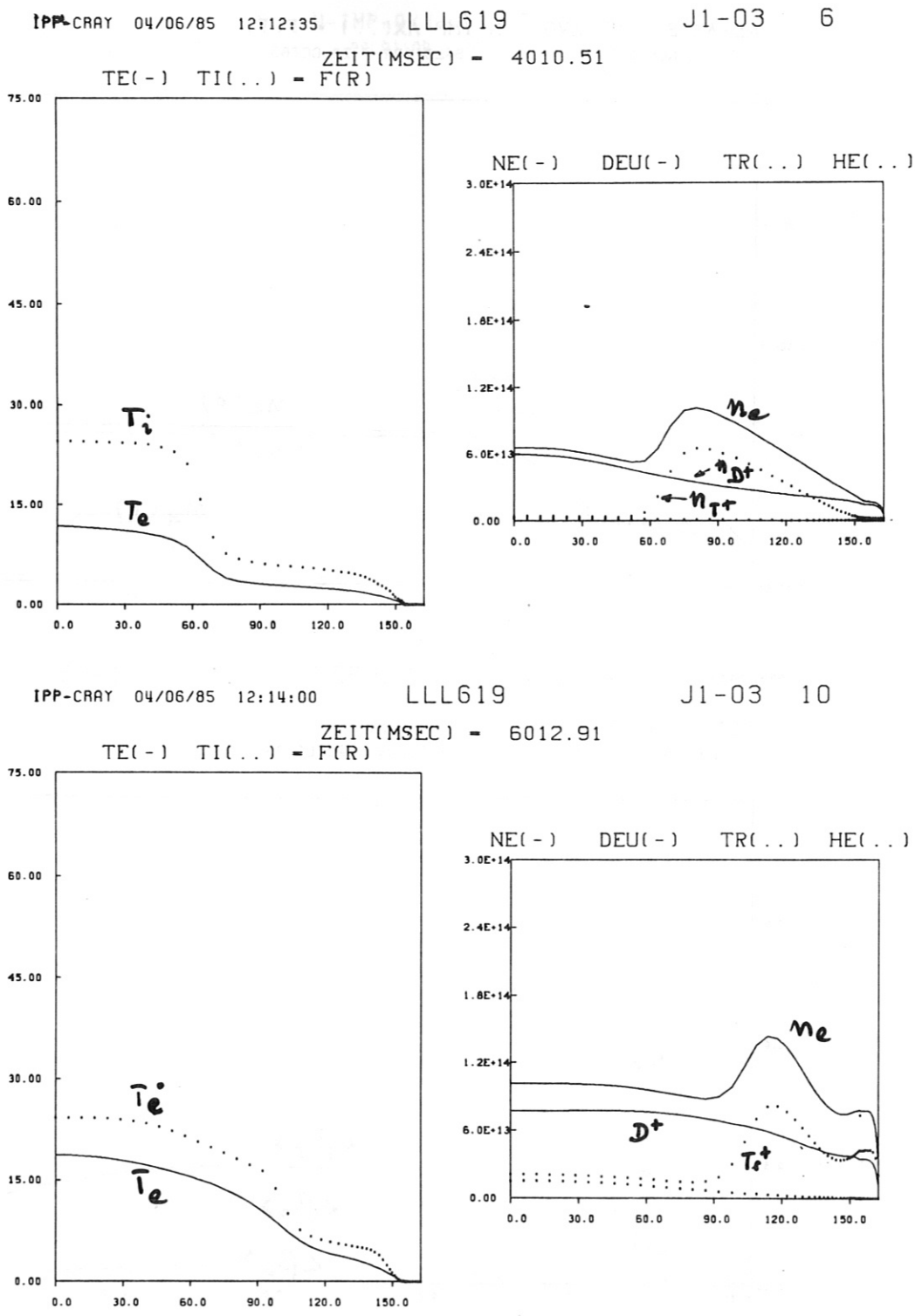

Fig. 12: Radial temperature and density distributions after the injection of the first and second pellets, (t_p = 4.0 s and 5.99 s, respectively) for the 80 keV/1.7 kA/3.0 s NB pulse case.

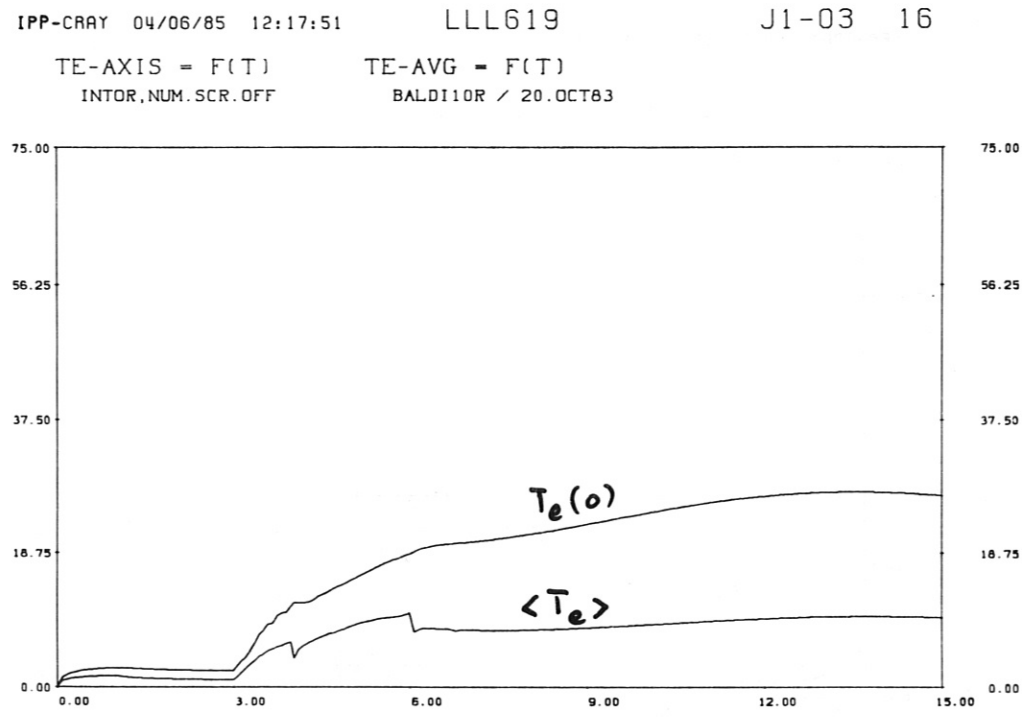

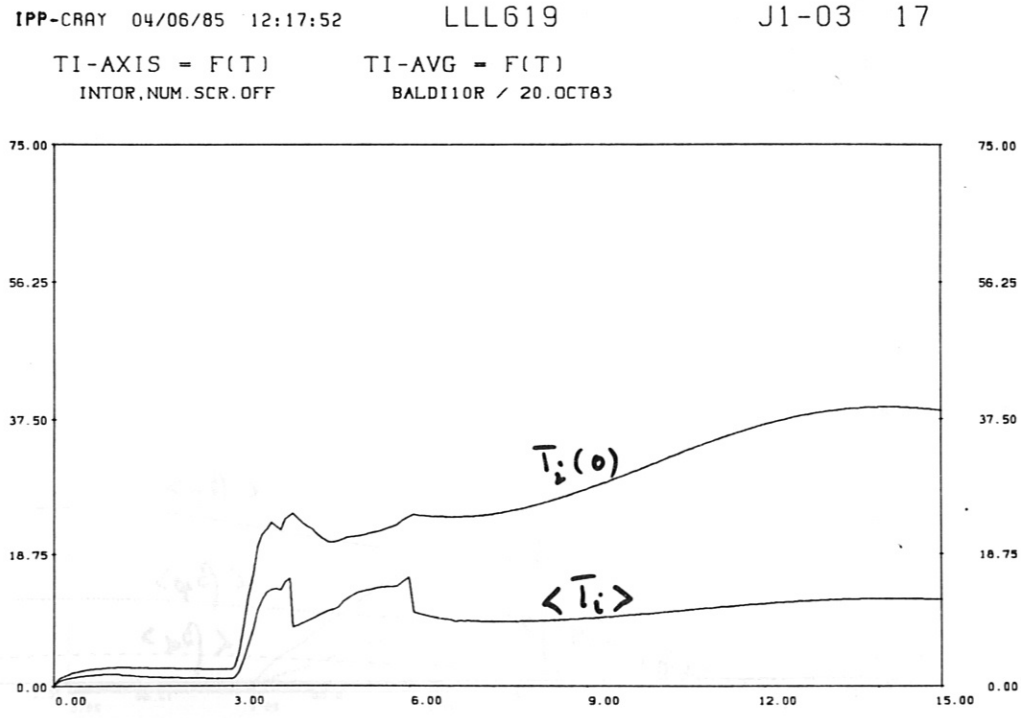

Fig. 13: Temporal variations of the electron and ion temperatures during density ramp-up by pellet injection for the 80 keV/1.7 kA/3.0 s NB pulse case.

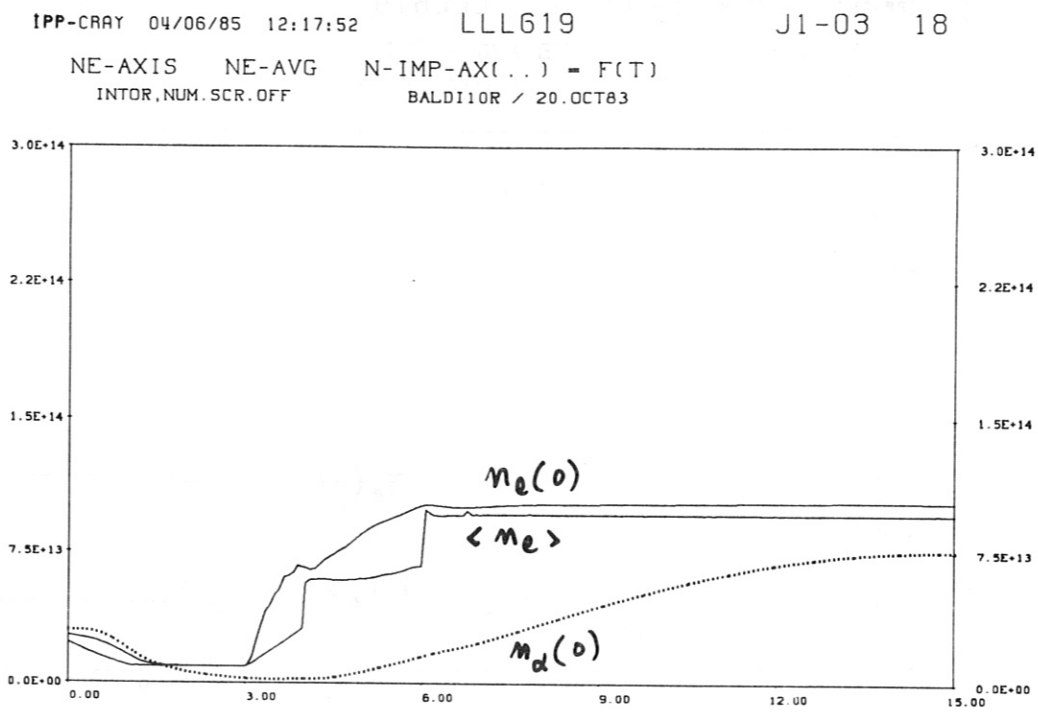

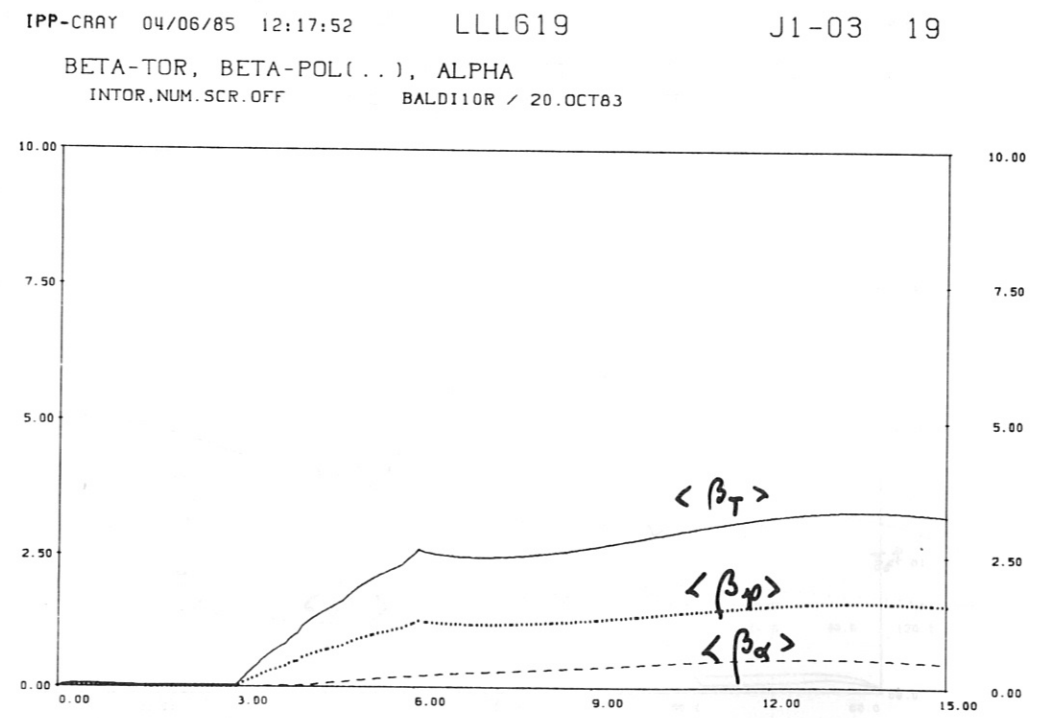

Fig. 14: Temporal variations of the electron and alpha particle densities and of the beta values during density ramp-up by pellet injection for the 80 keV/1.7 kA/3.0 s NB pulse case.

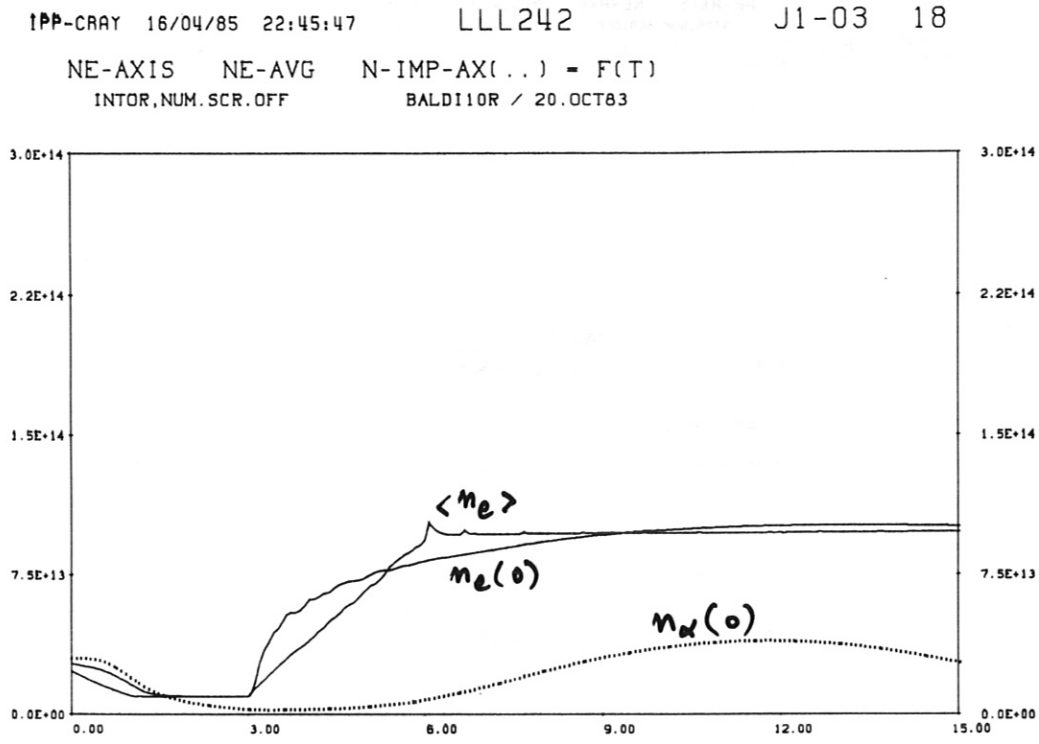

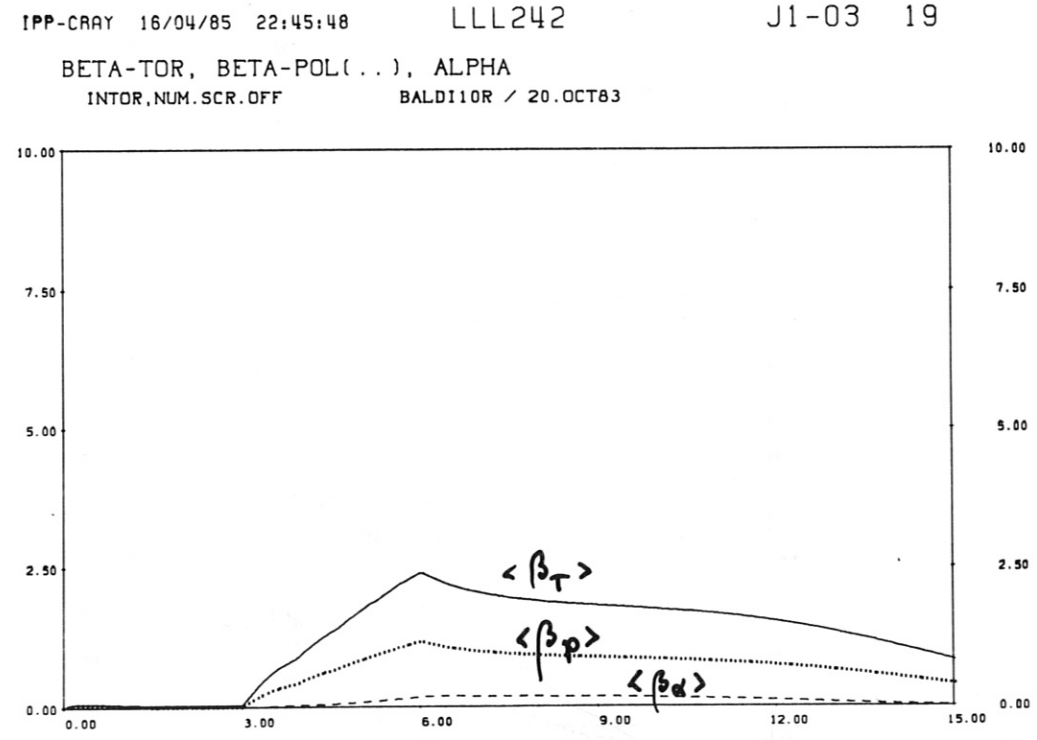

Fig. 15: Temporal variations of the electron and alpha particle densities and of the beta values for the reference discharge (density ramp-up by gas puffing) of the 80 keV/1.7 kA/3.0 s NB pulse case.

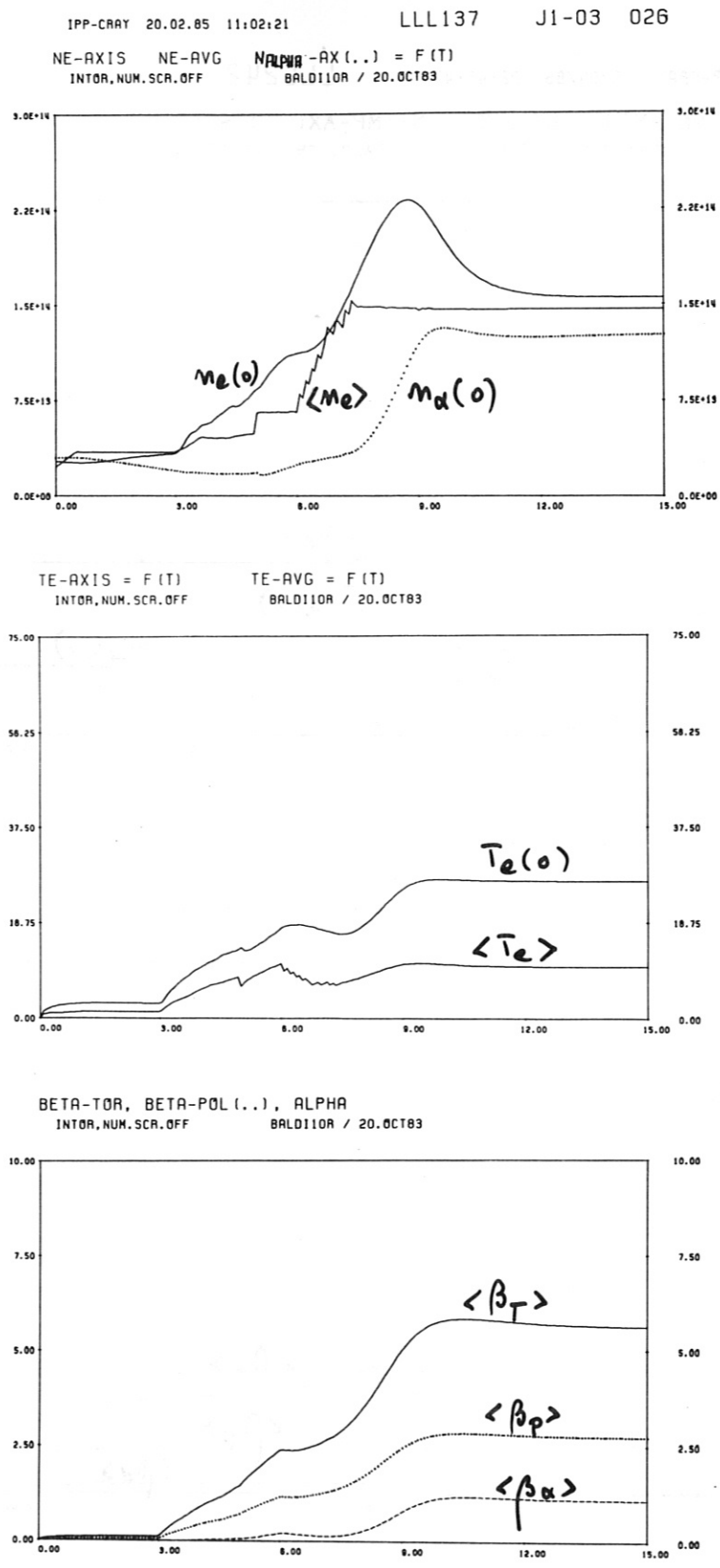

Fig. 16: Density ramp-up by a string of pellets: NB pulse: 100 keV/1.11 kA/3 s. Pellets: r_p = 0.25 cm, $v_{inj} \approx$ 3200 m/s. The first three pellets are T_2 pellets, the rest D_2 and T_2 pellets alternatingly.

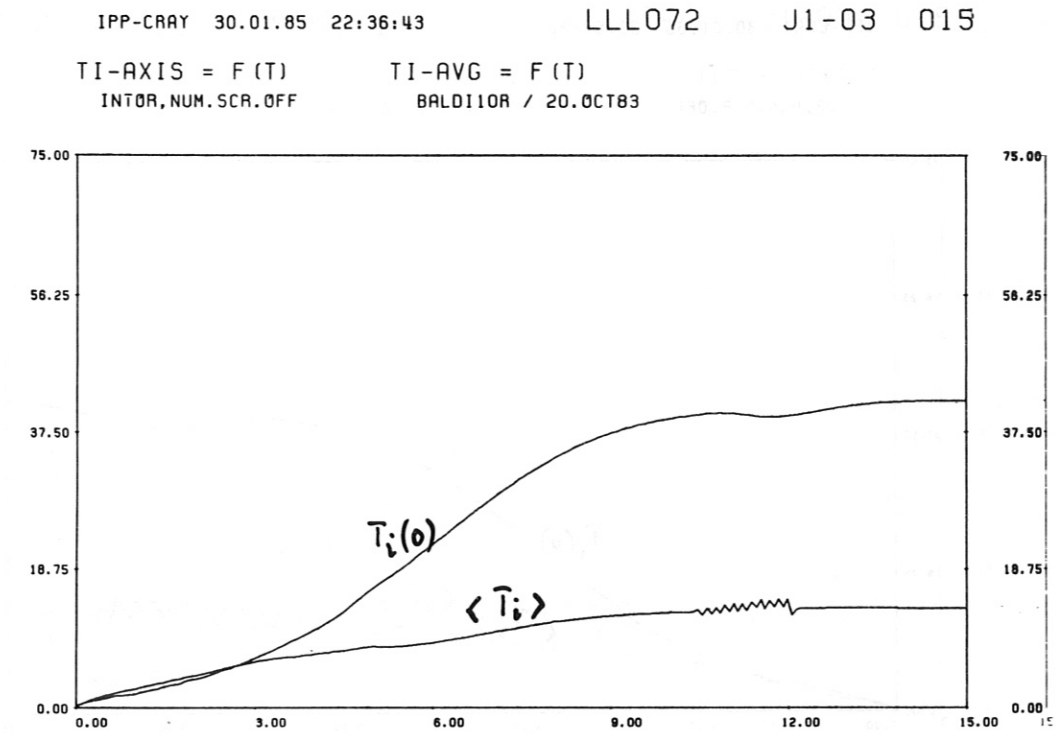

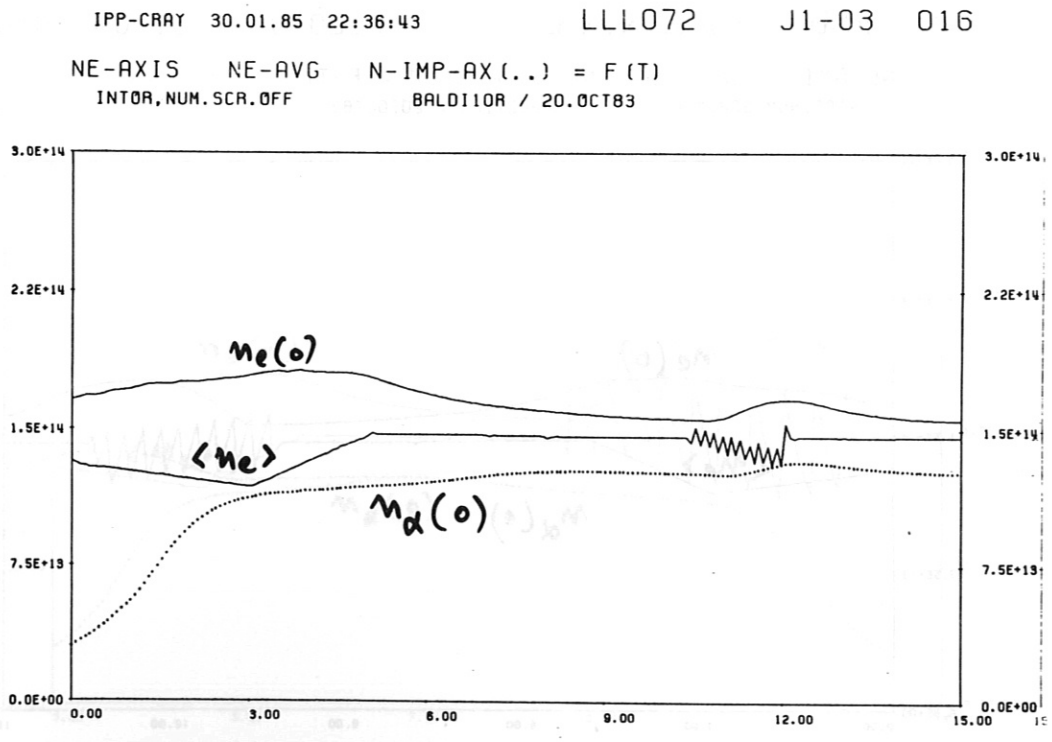

Fig. 17: Continuous fuelling: temporal variations of T_i and n_e for r_p = 0.26 cm, f_p = 6.7 s^{-1}, and $v_{inj} \approx$ 1600 m/s. (Neutral gas shielding ablation model.)

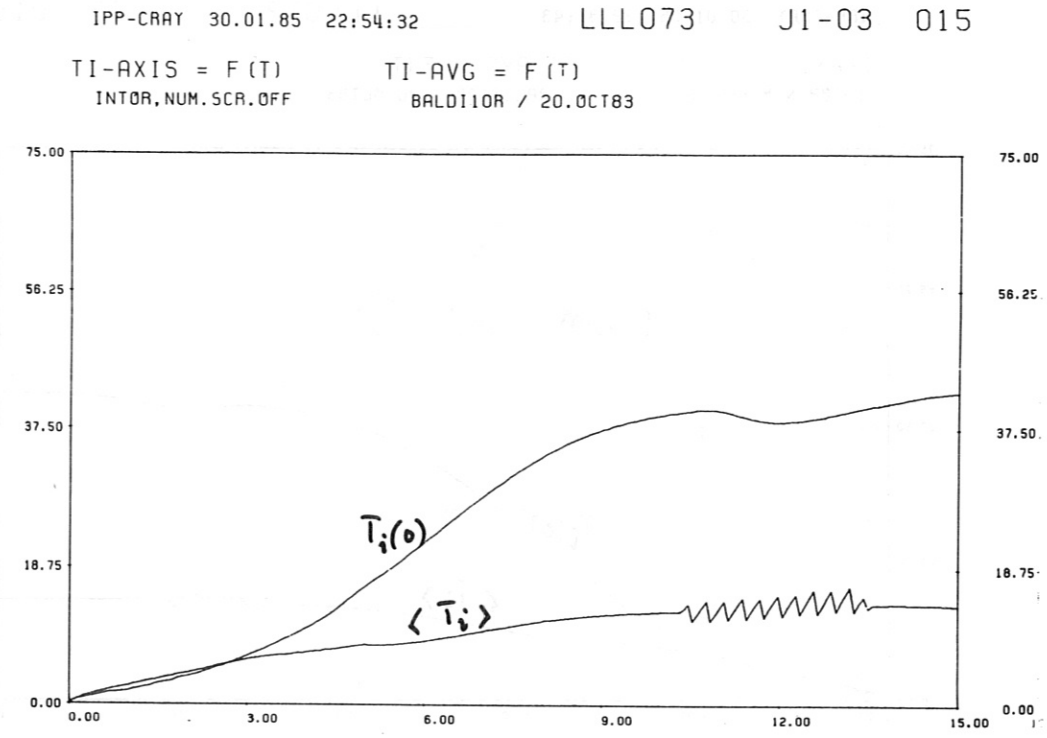

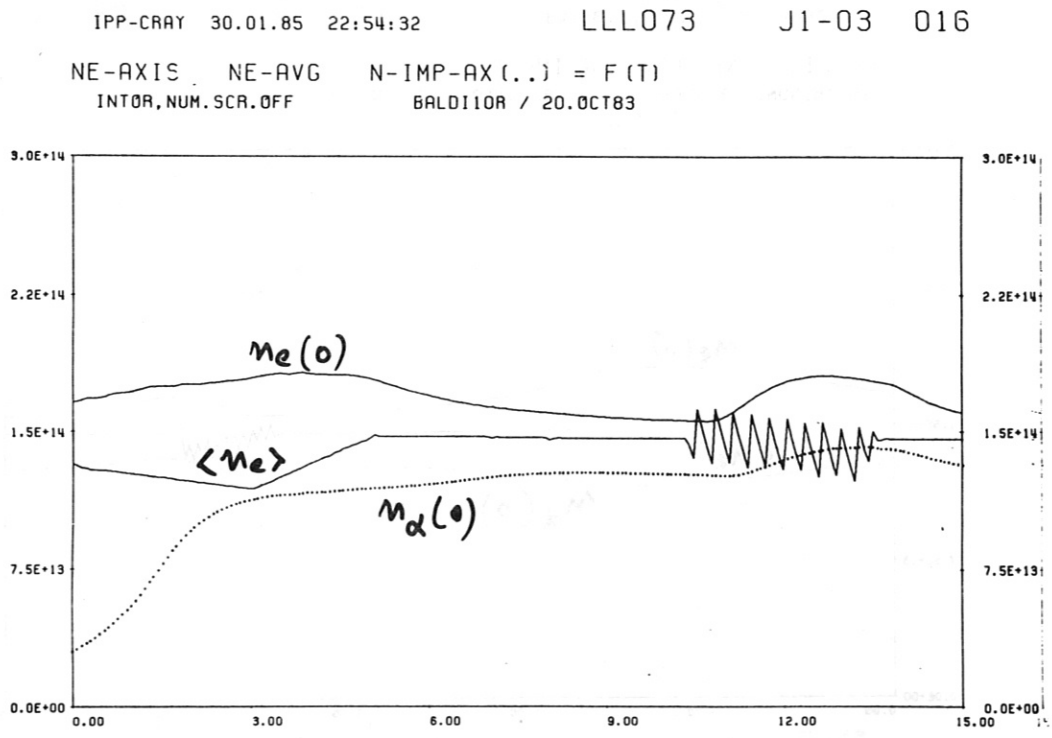

Fig. 18: Continuous fuelling: temporal variations of T_i and n_e for r_p = 0.33 cm, f_p = 3.3 s^{-1}, and $v_{inj} \approx$ 1600 m/s. (Neutral gas shielding ablation model.)

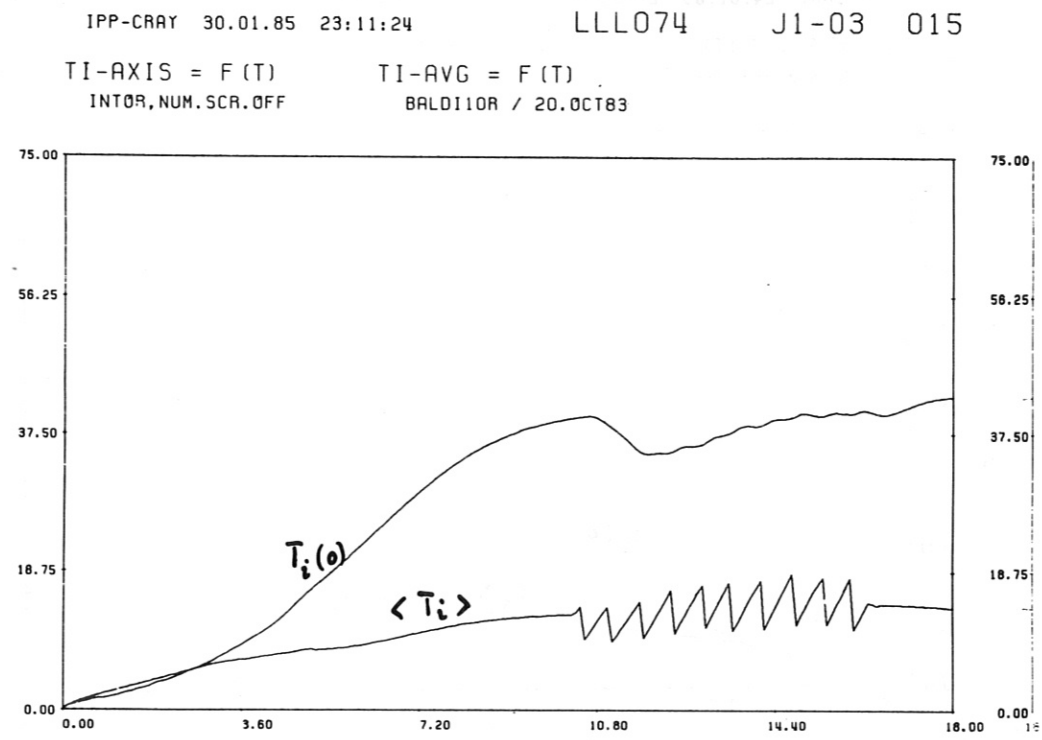

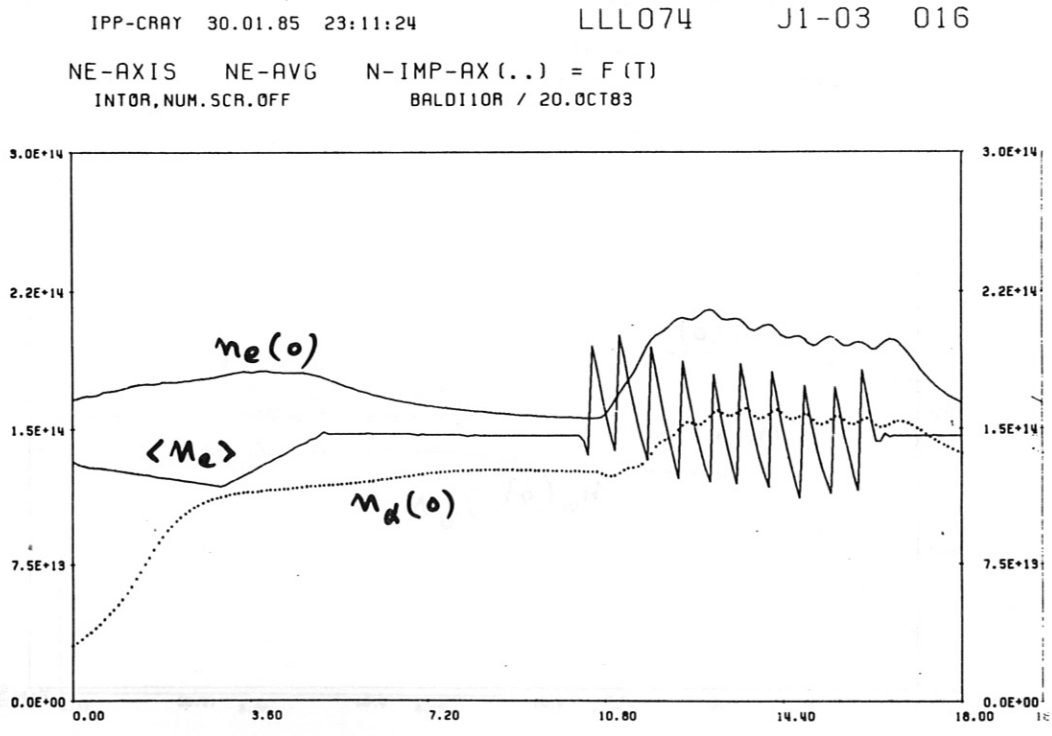

Fig. 19: Continuous fuelling: temporal variations of T_i and n_e for r_p = 0.42 cm, f_p = 1.7 s^{-1}, and $v_{inj} \approx$ 1600 m/s. (Neutral gas shielding ablation model.)

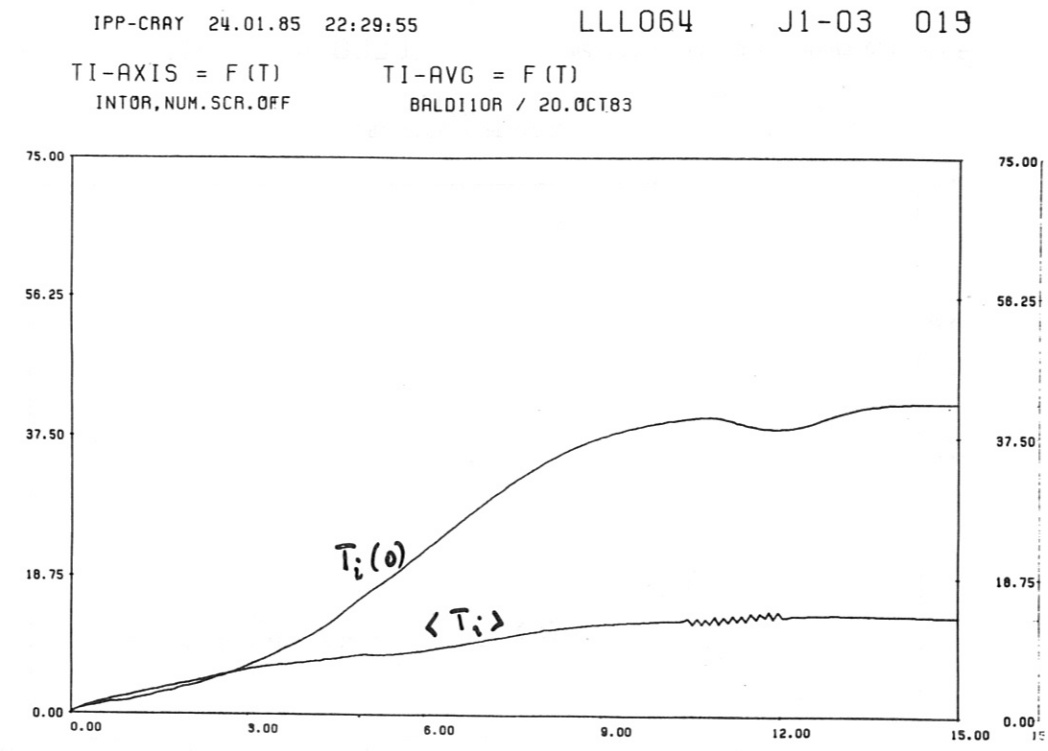

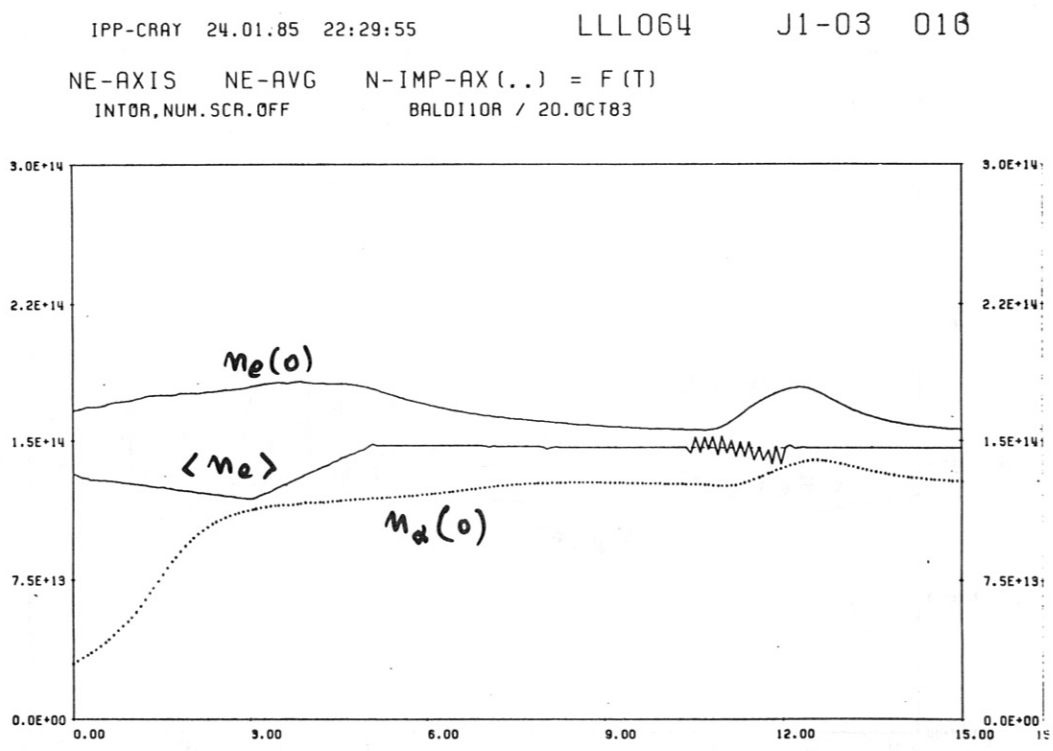

Fig. 20: Continuous fuelling: temporal variations of T_i and n_e for r_p = 0.26 cm, f_p = 6.7 s^{-1}, and $v_{inj} \approx$ 3200 m/s. (Neutral gas shielding ablation model.)

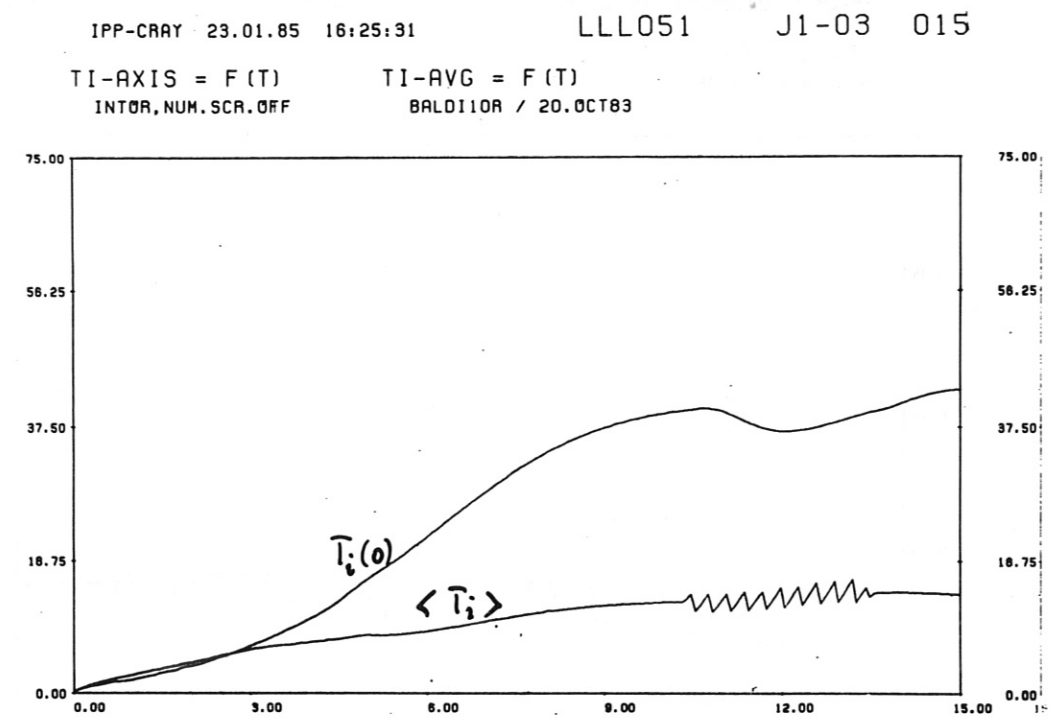

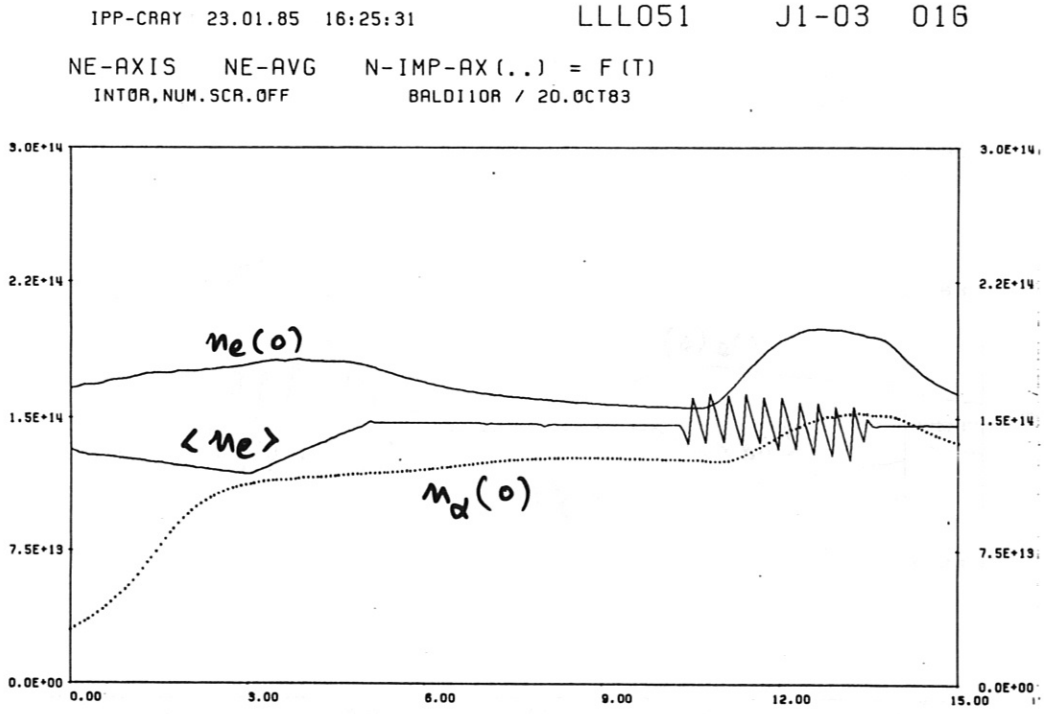

Fig. 21: Continuous fuelling: temporal variations of T_i and n_e for r_p = 0.33 cm, f_p = 3.3 s^{-1}, and $v_{inj} \approx$ 3200 m/s. (Neutral gas shielding ablation model.)

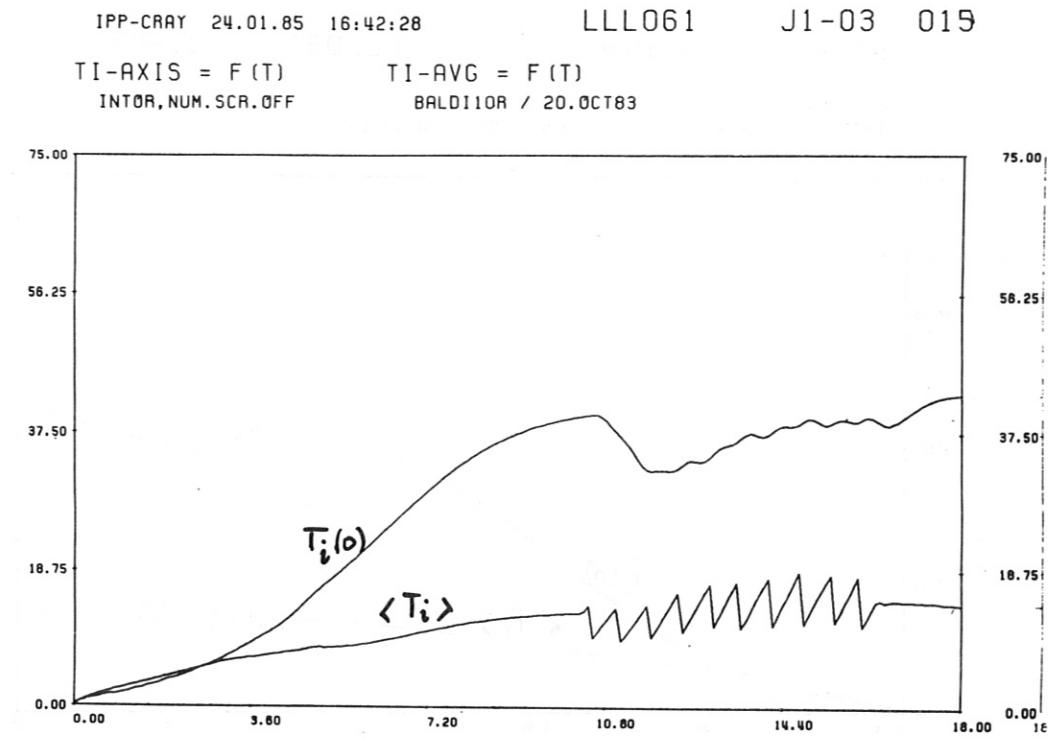

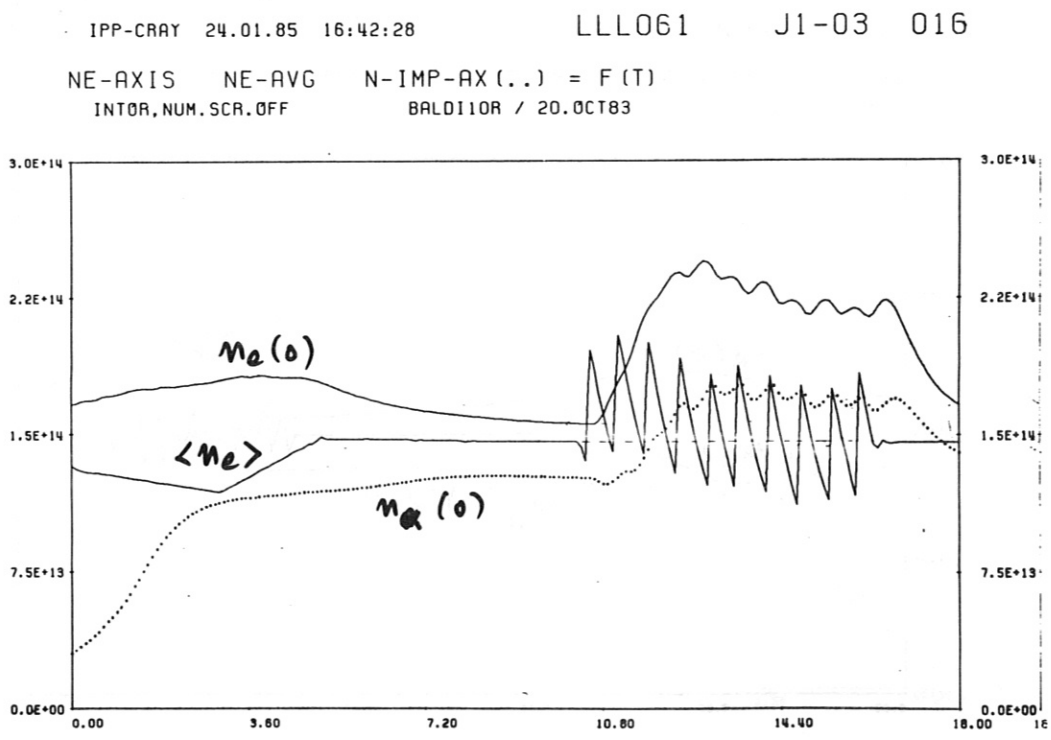

Fig. 22: Continuous fuelling: temporal variations of T_i and n_e for r_p = 0.42 cm, f_p = 1.7 s^{-1}, and $v_{inj} \approx$ 3200 m/s. (Neutral gas shielding model.)

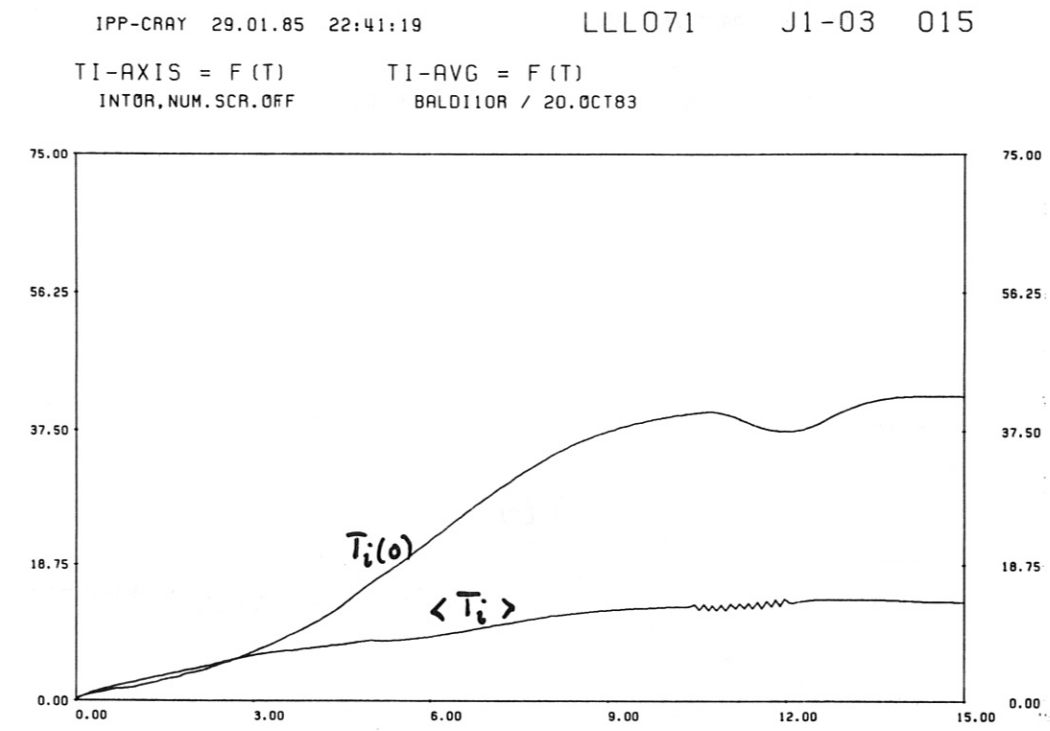

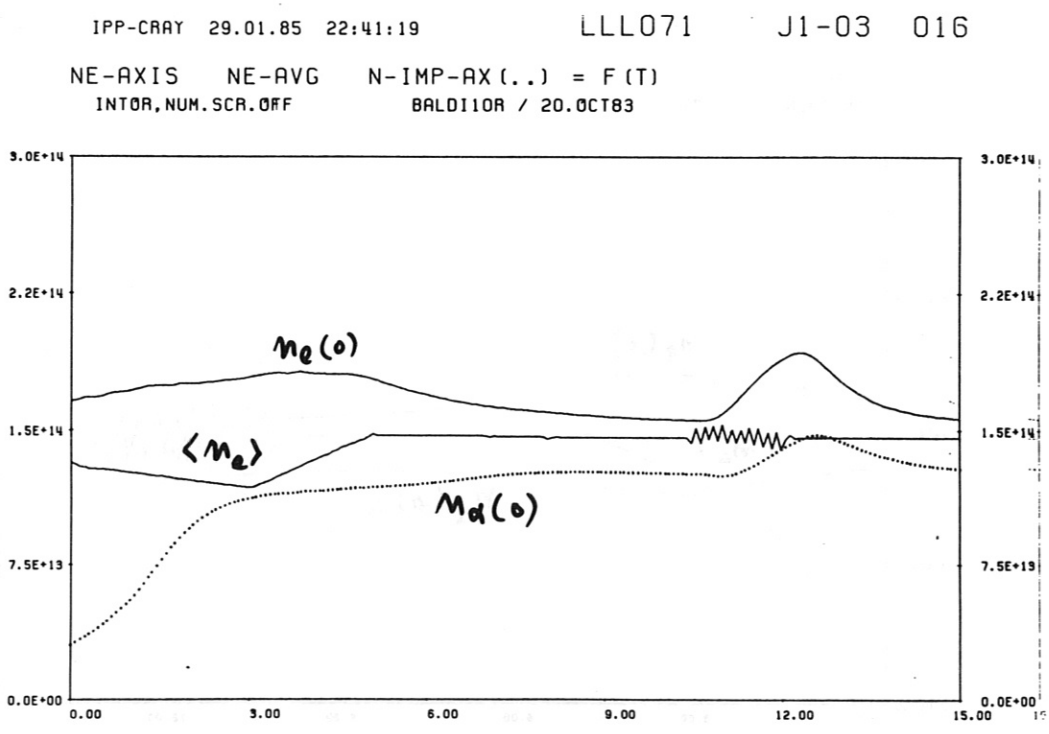

Fig. 23: Continuous fuelling: temporal variations of T_i and n_e for r_p = 0.26 cm, f_p = 6.7 s^{-1} and $v_{inj} \approx$ 1600 m/s. (Magnetic shilding approximation.)

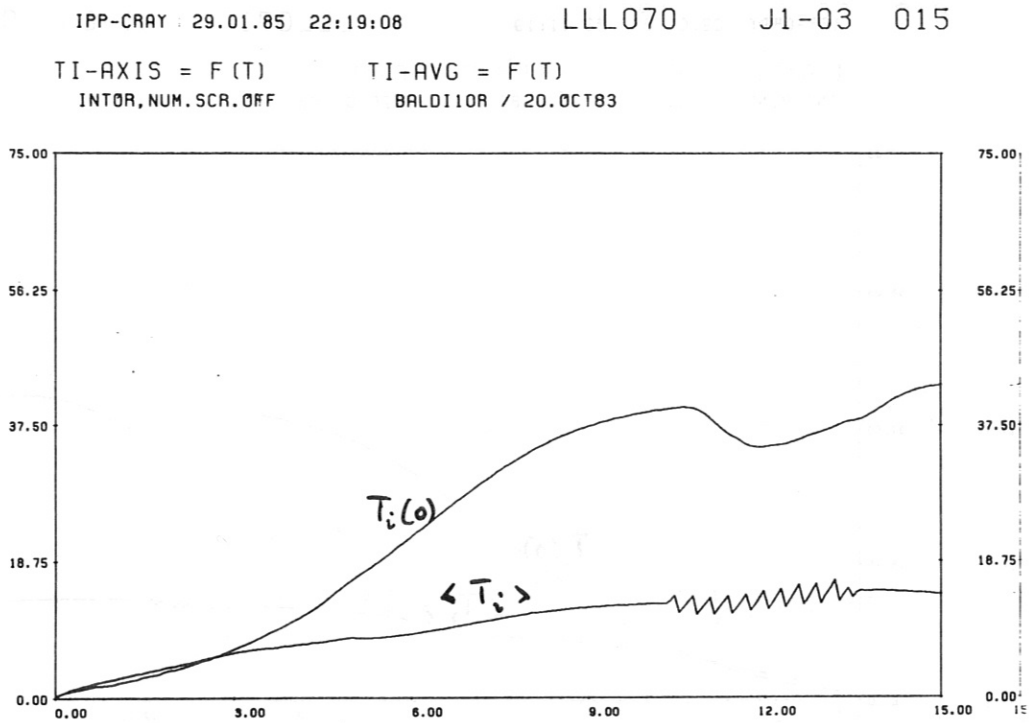

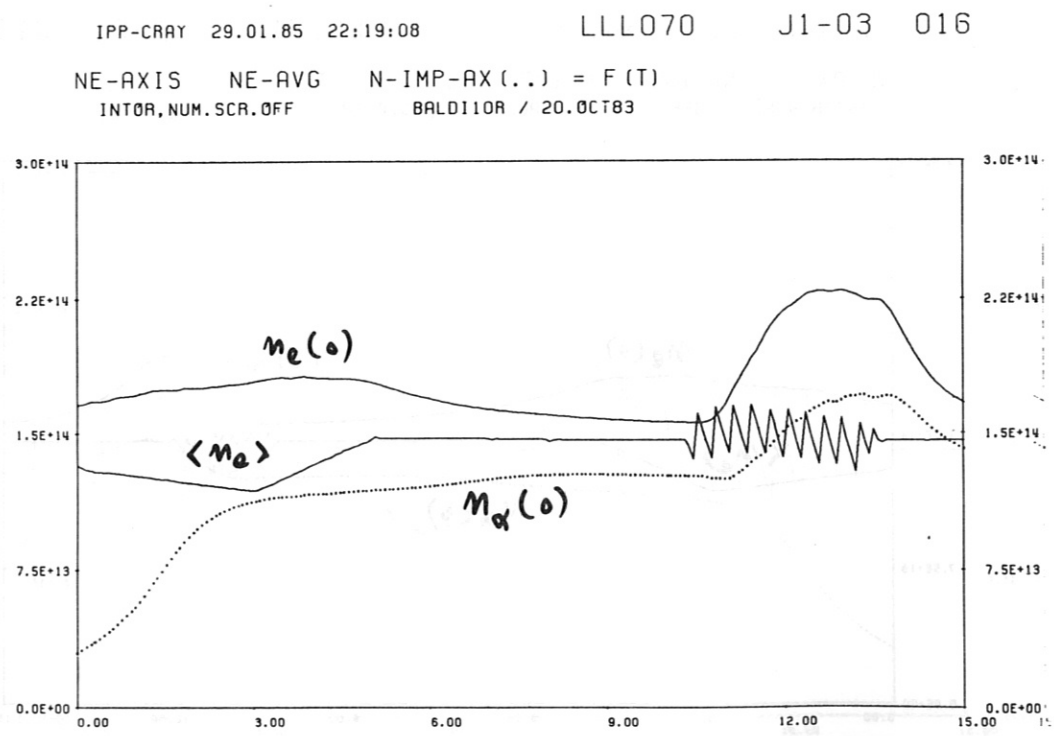

Fig. 24: Continuous fuelling: temporal variations of T_i and n_e for r_p = 0.33 cm, f_p = 3.3 s^{-1} and $v_{inj} \approx$ 1600 m/s. (Magnetic shielding approximation.)

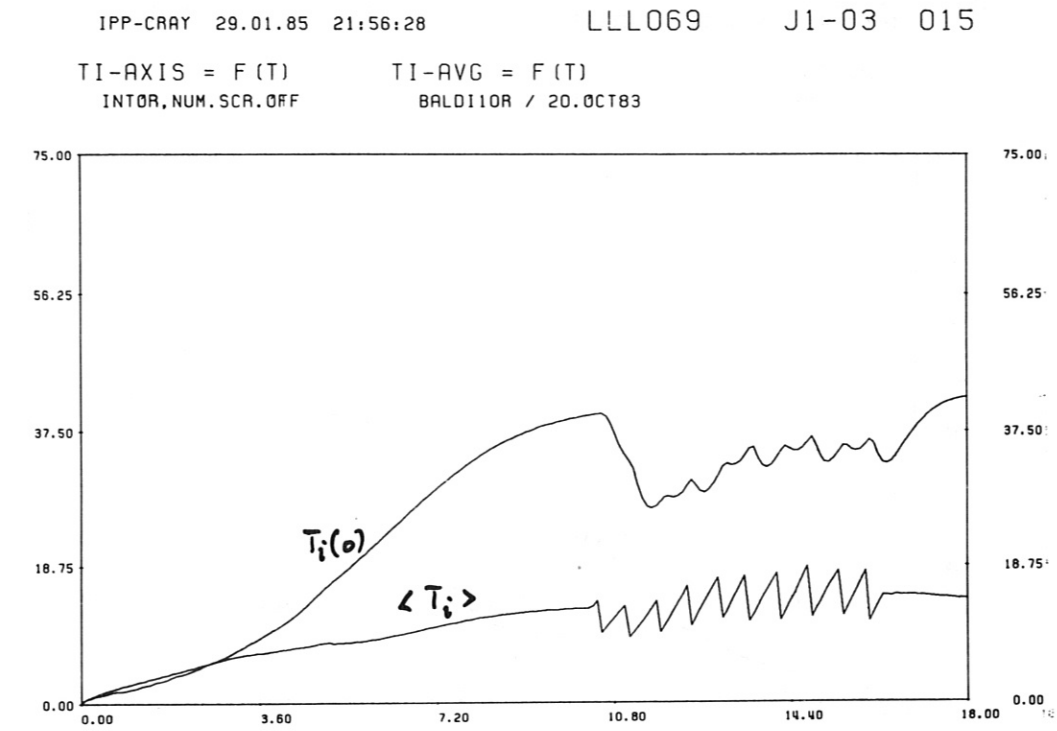

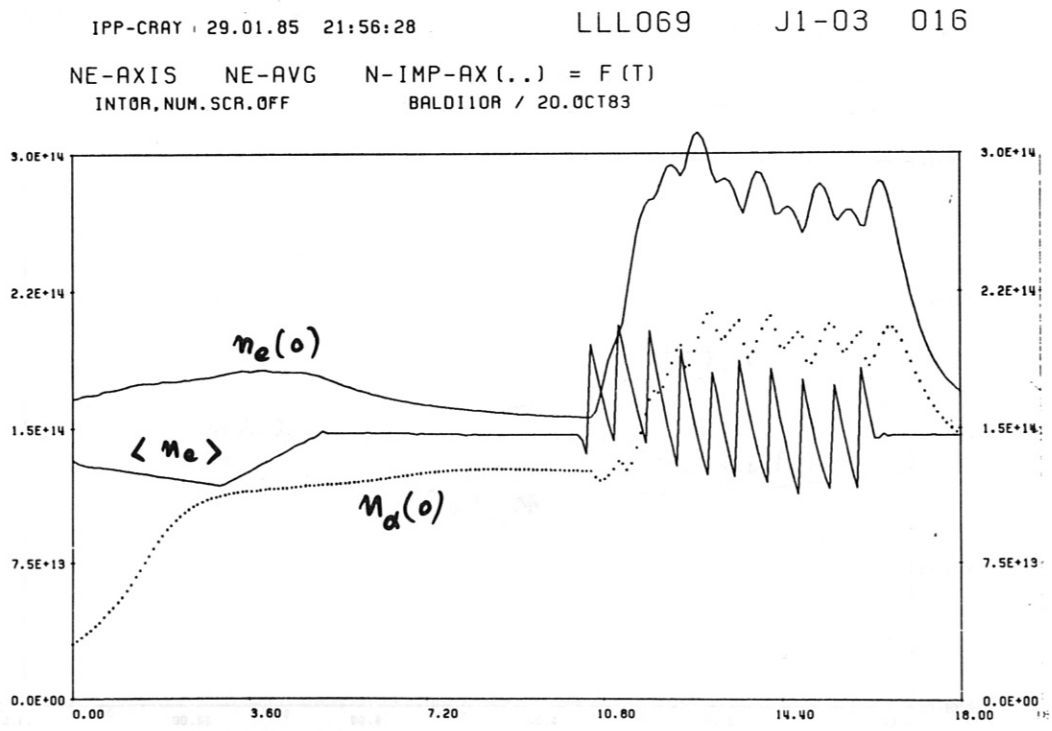

Fig. 25: Continuous fuelling: temporal variations of T_i and n_e for r_p = 0.42 cm, f_p = 1.7 s^{-1}, and $v_{inj} \approx$ 1600 m/s. (Magnetic shielding approximation.)

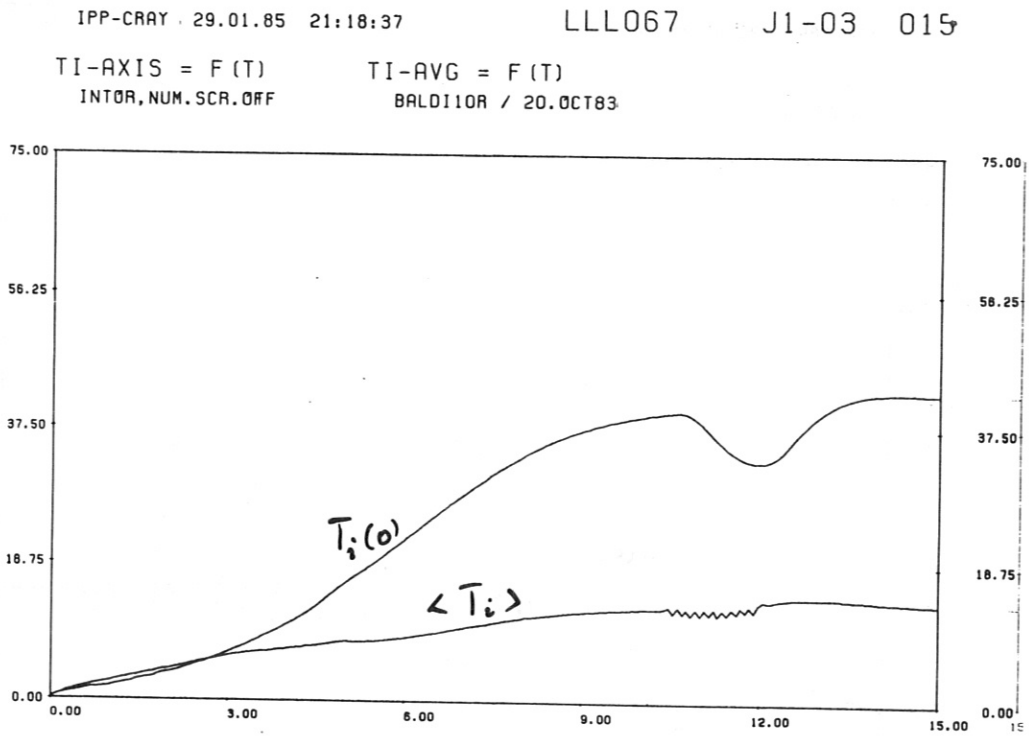

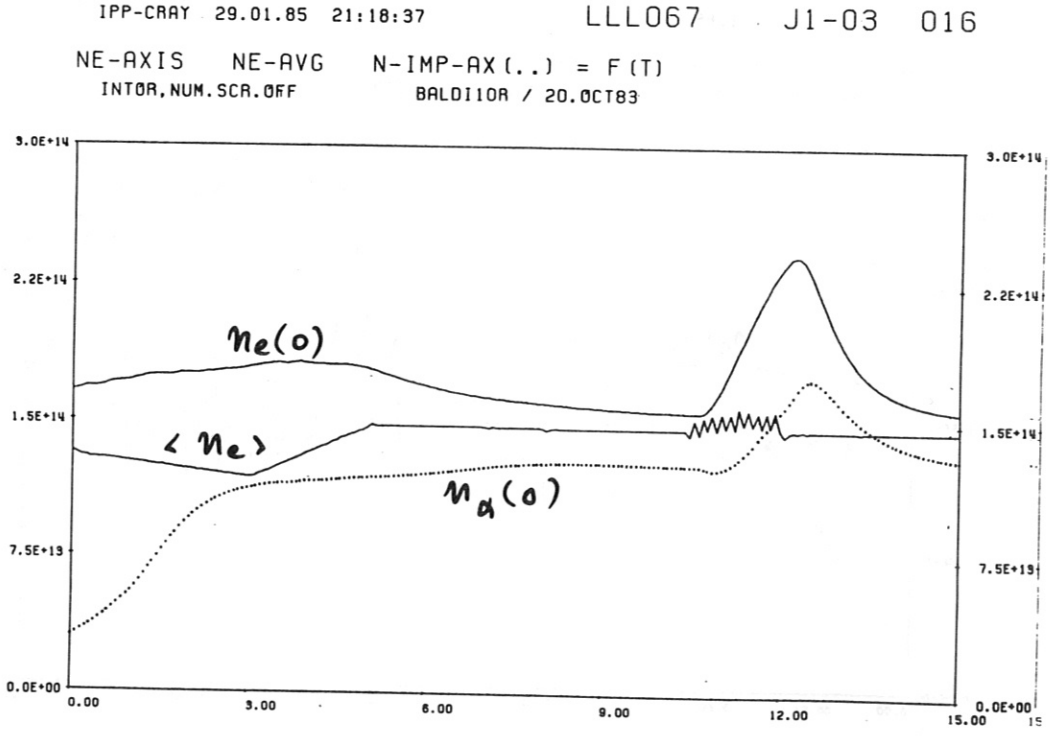

Fig. 26: Continuous fuelling: temporal variations of T_i and n_e for r_p = 0.26 cm, f_p = 6.7 s^{-1}, and $v_{inj} \approx$ 3200 m/s. (Magnetic shielding approximation.)

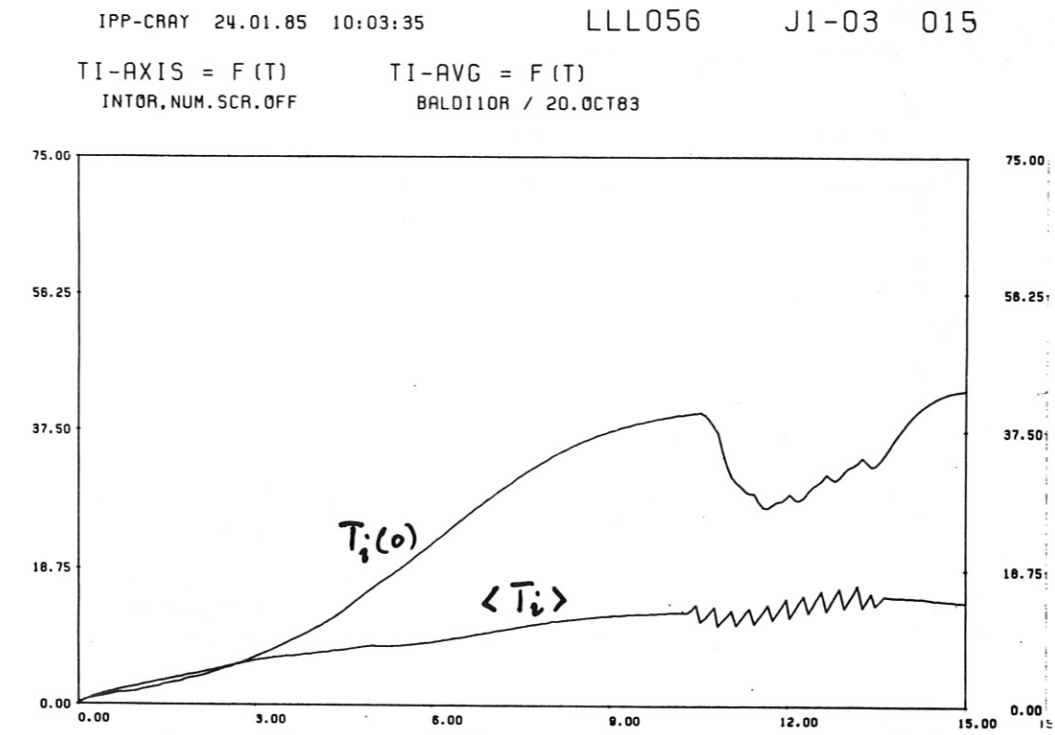

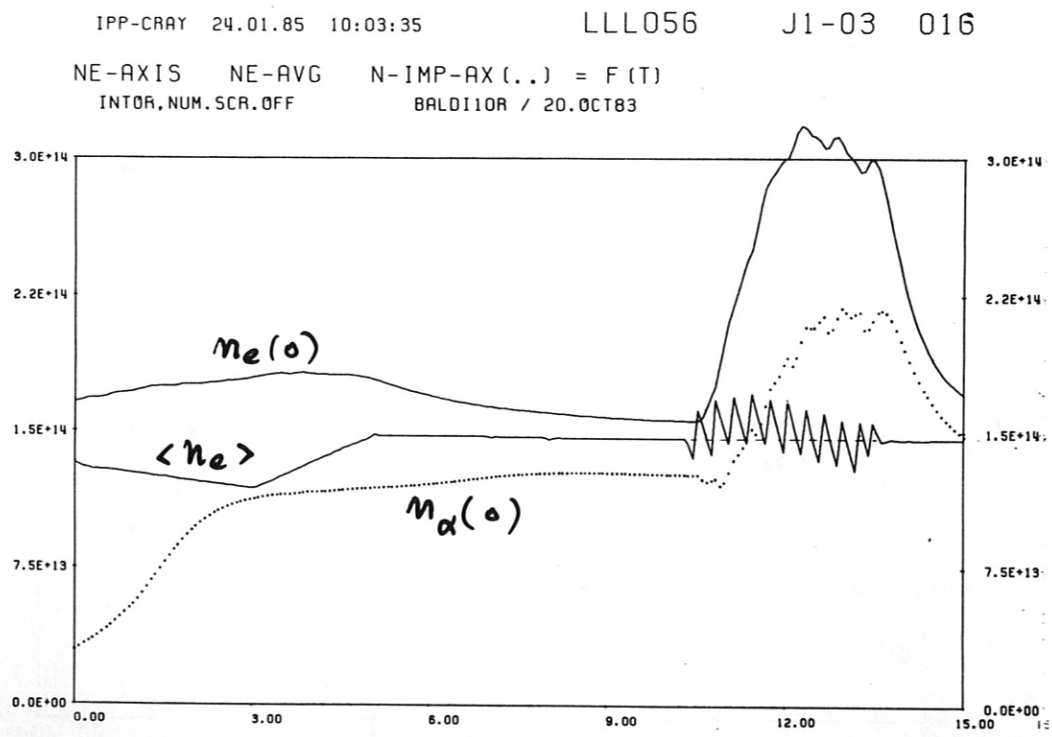

Fig. 27: Continuous fuelling: temporal variations of T_i and n_e for r_p = 0.33 cm, f_p = 3.3 s^{-1}. and $v_{inj} \approx$ 3200 m/s. (Magnetic shielding approximation.)

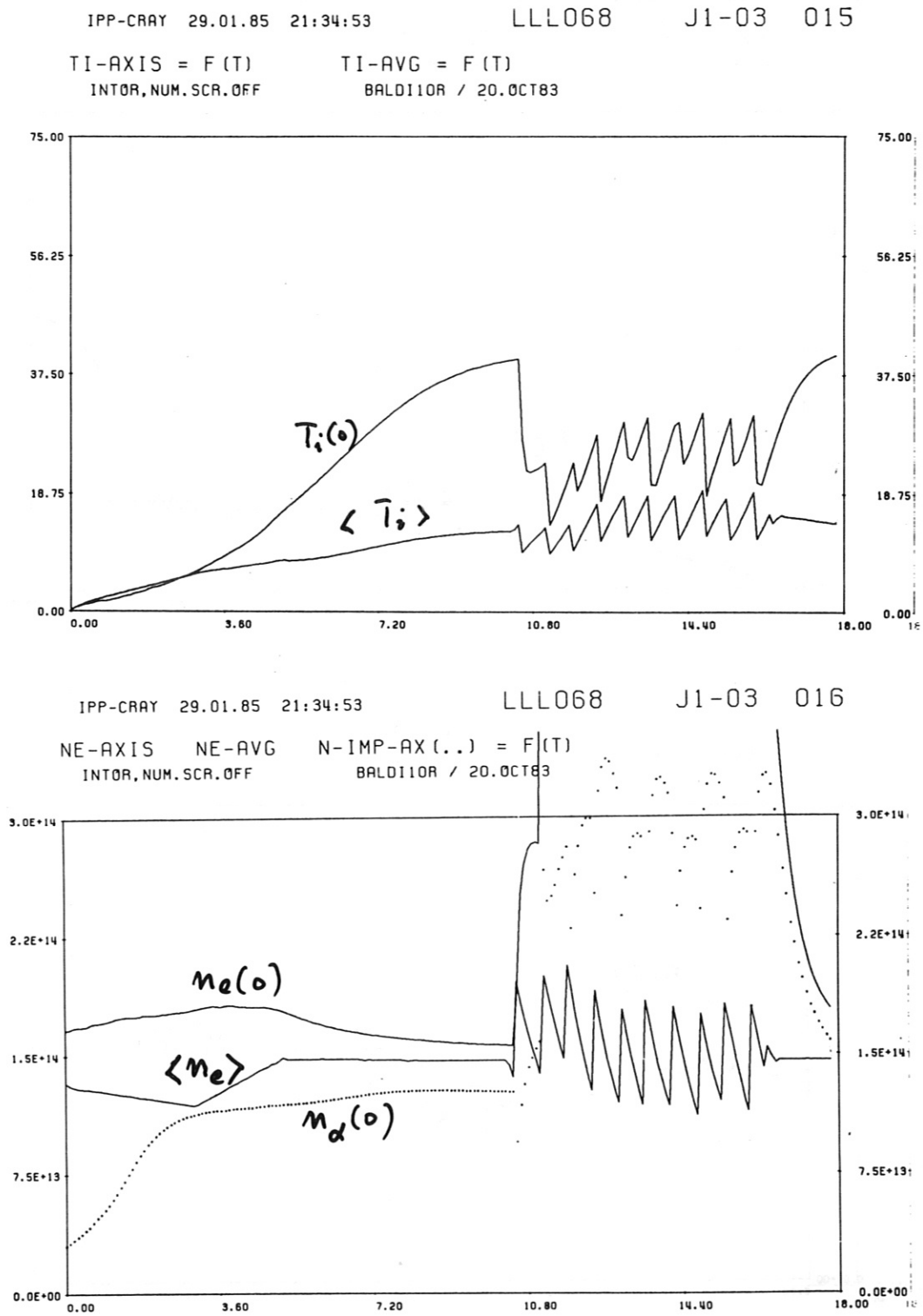

Fig. 28: Continuous fuelling: temporal variations of T_i and n_e for r_p = 0.42 cm, f_p = 1.7 s^{-1}, and $v_{inj} \approx$ 3200 m/s. (Magnetic shielding approximation.)